AD NUMBER

AD474103

LIMITATION CHANGES

TO:

Approved for public release; distribution is unlimited.

FROM:

**Distribution authorized to U.S. Gov't. agencies and their contractors;
Administrative/Operational Use; SEP 1965. Other requests shall be referred to Air Force Aero Propulsion Laboratory, Wright-Patterson AFB, OH 45433.**

AUTHORITY

AFAPL ltr dtd 12 Apr 1972

SECURITY MARKING

The classified or limited status of this report applies to each page, unless otherwise marked.
Separate page printouts MUST be marked accordingly.

THIS DOCUMENT CONTAINS INFORMATION AFFECTING THE NATIONAL DEFENSE OF THE UNITED STATES WITHIN THE MEANING OF THE ESPIONAGE LAWS, TITLE 18, U.S.C., SECTIONS 793 AND 794. THE TRANSMISSION OR THE REVELATION OF ITS CONTENTS IN ANY MANNER TO AN UNAUTHORIZED PERSON IS PROHIBITED BY LAW.

NOTICE: When government or other drawings, specifications or other data are used for any purpose other than in connection with a definitely related government procurement operation, the U. S. Government thereby incurs no responsibility, nor any obligation whatsoever; and the fact that the Government may have formulated, furnished, or in any way supplied the said drawings, specifications, or other data is not to be regarded by implication or otherwise as in any manner licensing the holder or any other person or corporation, or conveying any rights or permission to manufacture, use or sell any patented invention that may in any way be related thereto.

DISCLAIMER NOTICE

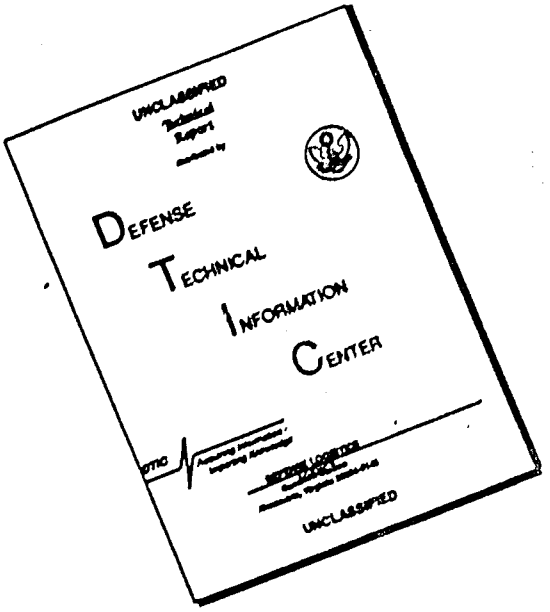

THIS DOCUMENT IS BEST QUALITY AVAILABLE. THE COPY FURNISHED TO DTIC CONTAINED A SIGNIFICANT NUMBER OF PAGES WHICH DO NOT REPRODUCE LEGIBLY.

AFAPL-TR-65-

HIGH SPECIFIC IMPULSE THERMAL ARC JET THRUSTOR TECHNOLOGY

Technical Report No. AFAPL-TR-65-

September 1965

Air Force Aero Propulsion Laboratory
Research and Technology Division
Air Force Systems Command
United States Air Force
Wright-Patterson Air Force Base, Ohio

Project No. 3141 , Task No. 314101

(Prepared under Contract No. AF 33(615)-1579
by Electro-Optical Systems, Inc.,
A Subsidiary of Xerox Corporation
Pasadena, California)

NOTICES

When US Government drawings, specifications, or other data are used for any purpose other than a definitely related government procurement operation, the government thereby incurs no responsibility nor any obligation whatsoever; and the fact that the government may have formulated, furnished, or in any way supplied the said drawings, specifications, or other data is not to be regarded by implication or otherwise, as in any manner licensing the holder or any other person or corporation, or conveying any rights or permission to manufacture, use, or sell any patented invention that may in any way be related thereto.

This document may not be reproduced or published in any form in whole or in part without prior approval of the Government. Since this is a progress report, the information herein is tentative and subject to changes, corrections and modifications.

FOREWORD

The work summarized in this Interim Report is being carried out for the Aero Propulsion Laboratory of the Air Force Research and Technology Division. The program is directed by the Electric Propulsion Technology Section headed by Capt. Paul E. Peko. Mr. Paul D. Lindquist is the Contract Technical Monitor.

The work is being performed at Electro-Optical Systems, Inc., in the Fluid Physics Division under the general management of Dr. E. L. Katz. Dr. G. L. Cann, Plasma Physics Department Manager, and Mr. R. A. Moore are principal investigators.

The report was prepared by Dr. G. L. Cann, Mr. R. A. Moore, Dr. P. F. Jacobs and Mr. L. R. Gallagher. The authors gratefully acknowledge the analytic contributions of Mr. R. L. Harder and the contributions of Messrs. C. H. Giltner, S. Snider, D. Etheridge, R. Swope, T. Jacobson and E. G. Doty to the design, fabrication, and experimental efforts.

The secondary report number assigned by Electro-Optical Systems, Inc. is 5090-IR-2. This report covers work accomplished during the period 1 April through 30 September 1965.

ABSTRACT

The objective of this program is to develop the technology of efficient electric arc jet thrustors for high specific impulse and long life. It is aimed particularly at power levels up to 300 kw, specific impulses between 1500 and 4000 seconds, and overall efficiency greater than 60 percent for durations of about 500 hours.

The approach combines analytical and experimental research to investigate and develop thrustors using lithium and other alkali metals as the propellant. The alkali metals have the advantage of high frozen-flow efficiency compared to gaseous propellants used in previous arc jet work. The use of lithium in this specific impulse range requires particle energies which are unattainable by the electrothermal arc-heating process. Thus, it is necessary to employ, in addition, electromagnetic acceleration mechanisms.

In the present approach a solenoidal magnetic field with a strength of several kilogauss is applied coaxial with an axially symmetric electrode system. The magnetic field forces the arc discharge to extend several jet diameters downstream of the electrodes and induces azimuthal Hall currents which are instrumental in containing and accelerating the plasma. The principal accelerating mechanism is thought to be the conversion of rotational kinetic energy of the bulk plasma to directed kinetic energy as the plasma flows out of the arc discharge region along the magnetic field lines.

In the reporting period a thrustor was tested in a high vacuum (10^{-7} torr) with lithium as a propellant, an identical thrustor was evaluated with potassium as the propellant with a wide variation of operating parameters, and improvements were made to the alkali metal feed system and the thrust measurement system. The high-vacuum tests essentially duplicated the performance of the lithium thrustor (I_{sp} = 5000 sec, η_T = 53 percent) measured at the higher pressure of 10^{-3} torr during a 10-hour endurance test. The efficiency and maximum specific impulse of the thrustor with potassium were lower than with lithium.

CONTENTS

ILLUSTRATIONS

LIST OF SYMBOLS

B	Magnetic field strength
B_o	Magnetic field strength on axis at anode
B_z	Axial component of magnetic field strength
E_r	Radial component of electric field
$\|e\|$	Absolute charge of electron
F_A	Bellows actuator force
F_S	Bellows spring force
I	Current
I_A	Arc current
I_{sp}	Specific impulse
k	Boltzmann constant
M	Molecular weight
m	Mass
m_a	Atomic (or ionic) mass
$\dot{m}_A$	Mass flow through anode
$\dot{m}_c$	Mass flow rate out of cathode jet
$\dot{m}$	Mass flow rate
P_I	Arc power input
P_c	Cathode power
P_{tip}	Cathode power loss with attachment at the tip of a cone
P_{ring}	Cathode power loss with attachment on a cylindrical ring
P_A	Power lost to anode
q	Heat flux
R	Cathode radius
R_c	Cathode jet radius at the mean position of current crossover
R_{A_o}	Anode radius

LIST OF SYMBOLS (contd)

R_{C_o}	Arc radius at cathode
r	Radial coordinate
t	time
T	Thrust or temperature
T_a	Gas temperature entering anode sheath
T_c	Exit temperature of gas from cathode jet
V	Voltage or volume
V_A	Potential drop along anode sheath or arc voltage
V_{T-A}	Voltage between tank and anode
V_{T-C}	Voltage between tank and cathode
V_I	First ionization potential
V_{II}	Second ionization potential
v	Azimuthal velocity
w	Axial velocity
$\bar{w}$	Average axial velocity of gas near anode
x	$(L_{max} - L)$ = displacement of bellows
γ	Ratio of specific heat capacities
η_T	Thrust efficiency
μ_o	Permeability of vacuum
ρ	Density
Ψ	$\frac{\lvert e \rvert \dot{m}}{m_a I}$
θ	Included angle of cathode conical tip
δ	Half-width of ring attachment

1. INTRODUCTION

This report summarizes the results obtained during the first 6 months of the second year of a three-year program which began in April 1964. This Interim Report covers the period 1 April to 30 September 1965. The program objective is the development of arc jet technology to the point where it will be possible to build plasma thrustors capable of the following performance:

Power Input:	up to 300 kw
Specific Impulse:	1500 to 4000 seconds
Overall Efficiency:	greater than 60 percent
Lifetime:	500 hours

The approach has been to experimentally and analytically investigate thrustors which rely predominantly on Hall currents to accelerate alkali metal propellants. This report presents performance measurements with lithium and potassium propellants, results of analyses of the acceleration and electrode mechanisms, and descriptions of test equipment and measurement techniques. The experimental results include measurement of performance with lithium at chamber pressure levels down to 10^{-7} torr and a study of the effects of magnetic field strength, mass-flow-rate, test chamber pressure, and arc current on the performance with potassium.

The present investigation of alkali-metal arc jets was begun after two types of electromagnetic arc jets had shown the capability to efficiently accelerate hydrogen to the specific impulse level of about 10,000 sec. In the first type (Ref. 1) the principal plasma acceleration forces result from the interaction between the applied arc current and the self-induced magnetic field. The second type (Refs. 2 and 3) relies on a strong applied magnetic field interacting with the applied arc current to generate Hall currents, which

have an important role in the plasma acceleration process. It is felt that the acceleration process in the second type is primarily the result of the conversion of rotational energy into directed kinetic energy. The rotation of the plasma about the thrustor axis is induced by the arc current crossing the applied magnetic field. The rotational motion is converted to axial motion as the plasma expands while flowing out along the applied magnetic field lines. The role of the Hall currents is that of confining the plasma to a flow path along the field lines during the expansion process.

The early hydrogen results logically led to the study of the potentially more efficient alkali metal propellants, beginning with lithium in the present program (Ref. 4). The hydrogen performance showed that the electromagnetic mechanisms could accelerate plasma to higher kinetic energy per particle than had previously been achieved in electrothermal devices, and to sufficiently high energies that heavier propellants could be used. Clearly, the best choices among heavy propellants are the alkali metals because of their low ionization losses and ease of storage during long missions. In the present program the performance capabilities of lithium and potassium have been investigated. In a separate program* at this laboratory sodium was also tested. Results from similar, more recent, investigations with alkali-metal arc jets at other establishments have begun to appear. These include lithium and cesium (Ref. 5), and potassium (Ref. 6).

*NASA Contract NAS 3-5909

2. SUMMARY

The analytical and experimental research aimed at developing the technology of high specific impulse arc jets was continued during the reporting period. The research in this period was concentrated on:

1. Testing a lithium arc jet, which was developed and endurance tested during the earlier first phase of this program (Ref. 4), in a high vacuum test chamber to determine the effect of pressure level on the thrust and efficiency.
2. Evaluating the performance of the lithium arc jet using potassium as the propellant. The effects of operating parameters — current, magnetic field strength, mass-flow-rate, and test chamber pressure — were determined.
3. Improving the accuracy and reliability of the principal measurement systems (thrust balance and propellant feed system) necessary for this research.
4. Analytically investigating the significant physical processes occurring in the high specific impulse arc jet with emphasis on determining the predominant acceleration, energy loss, and electrode mechanisms.

The work throughout has been concerned with an arc jet concept which depends on acceleration of an alkali-metal plasma resulting from Hall-currents induced in the plasma. The Hall currents are induced by a strong (1-5 kilogauss) magnetic field applied to an arc established between coaxial electrodes.

Specific impulse and efficiency measured in the high vacuum tests at a chamber pressure level of $2 - 3 \times 10^{-7}$ torr were in the range of 4000 to 4500 seconds and 45 to 51 percent, respectively with a 10 kw thrustor. This performance compares closely with that of the 10-hour

endurance test in which a specific impulse of 5000 sec and an efficiency of 53 percent were measured at a pressure level of 6×10^{-3} torr in a different test chamber. The specific impulse at the lower pressure was lower because the mass-flow-rate was slightly higher than in the higher pressure test. For both tests the current was held constant at 250 amperes and the voltage was about 40 volts. These results seem to indicate that the pressure has little effect on thrustor performance below the range of 10^{-3} torr; however, the principal concern is mass entrainment rate, and additional tests are needed to verify that the entrainment rate at high-vacuum conditions is insignificant. It is possible that as the pressure is lowered and the entrainment rate per unit area decreases that the area of the acceleration region of the plasma increases.

With potassium propellant the arc jet had a maximum specific impulse of about 1600 seconds with an efficiency of about 30 percent. This is significantly lower than the 5000 sec and 50 percent measured with lithium. The poorer potassium performance is tentatively attributed to the lower plasma number density with potassium and lower second ionization potential.

Analysis of the plasma acceleration processes has led to the conclusion that the predominant acceleration mechanism is the conversion of energy in the azimuthal direction of plasma motion to axially directed kinetic energy as the plasma expands through the divergent magnetic field (i.e., magnetic nozzle). This azimuthal energy, which is predominantly in the ions, is due to the applied arc current crossing the applied magnetic field lines. This theory is consistent with the observed "anomaly" that the measured specific impulse is greater than that which corresponds to ions electrostatically accelerated through the potential difference of the electrodes. The analysis also properly predicts other experimentally observed trends; however, the final equations are approximate and the thrust

expression is in terms of the mean radius of the expanding plasma where the current crosses the magnetic field. This radius is a parameter which is dependent (in a presently unknown fashion) on other variables. Thus, a considerable amount of additional effort will be necessary before the analytic tools will be of full benefit to the thrustor design and development tasks.

The analysis of cathode phenomena has so far concentrated on the mechanism of energy transport to the cathode surface and the conduction of heat through the cathode tip. It has been concluded that there are primarily two possible modes of operation of a cathode in the Hall arc jet. These are a diffuse mode dominated by ion bombardment and a spot mode dominated by thermal conduction. Based on the assumption that the electron-emitting surface of the cathode operates at the melting point of the cathode, calculations of the heat flow through the cathode tip show that the lowest apparent power loss would be with the arc attached to the tip of a conical cathode. Since this is consistent with experimental observations with gaseous propellants, it is planned to test a means of forcing spot attachment with an alkali-metal propellant as the next step in the program.

Also in the realm of electrode mechanisms, an expression has been derived for the anode power loss in terms of the thrust produced and certain other parameters relating to the propellant flow, the molecular weight, and the arc current. Though this result is based on a simple model of the anode sheath, it is consistent with the trends of the measurements of anode power loss.

Along with the tasks of experimental and analytical study of the thrustors a continuing effort has been devoted to refining the techniques of the difficult measurements of thrust and mass-flow-rate. The bellows-type positive displacement feed system has been improved, by changes in operational procedure, precise calibration

measurements, and addition of a propellant vaporizer, to the point where precise measurements and reliable operation are more routine. In addition, design has been started on a modified high-capacity feed system needed for future endurance testing of the thrustors. The thrust balance is in the process of being modified so that electromagnetic tare forces and other extraneous forces can be reduced to an insignificant level. It is believed that this thrust measurement system will have exceptional accuracy and reliability for the testing of the future Hall arc jets.

3. THRUSTOR PERFORMANCE MEASUREMENTS

This section presents the results of experimental studies of high-specific-impulse electromagnetic arc jets conducted during the reporting period. The experiments were high-vacuum tests with lithium propellant, and performance evaluation and parametric study with potassium propellant. The thrustor configuration was the same for both of these investigations although different thrustors were used.

The performance parameters of primary interest are specific impulse and thrust efficiency. Specific impulse was calculated from the measured thrust and mass-flow-rate values using the following equation:

$$I_{sp} = \frac{T}{\dot{m}g} \tag{1}$$

Thrust efficiency was calculated from the measured arc power input, in addition to the measured thrust and mass-flow-rate:

$$\eta_T = \frac{T^2}{2\dot{m} P_I} \tag{2}$$

where

$$P_I = I_A V_A \tag{3}$$

It is noted that the power input in the above equation does not include:

1. Power dissipated in the magnet coil (about 22 kw at the maximum coil current of 1800 amperes);
2. Power required to operate the feed system, and
3. Power in the propellant where it enters the thrustor.

The coil power is not included because the development of low-power coils is beyond the scope of the work. The coil designs used were dictated by the criteria of maximum fabrication simplicity (i.e., low cost) and an optimum match to the voltage-current characteristics of an existing magnet power supply. Calculation shows that the same field could be produced with a power dissipation of only 3.3 kw by a coil of more efficient design. (See Ref. 4.) In the final evaluation of the performance capability of these thrustors, it is intended to include the coil power dissipation estimated to be possible in the space propulsion system.

3.1 High-Vacuum Tests of a Lithium Thrustor

The high-vacuum tests were conducted as one step in the process of determining the effect of test chamber pressure on thrustor performance so that the pressure level necessary for adequate space simulation can be assessed. A Model LAJ-AF-6D Lithium Arc Jet shown in Fig. 1 was tested in the Ion Engine 5' x 12' (5 ft dia by 12 ft long) vacuum chamber at pressures down to 2×10^{-7} torr. For the tests in the 5' x 12' chamber the thrustor and lithium feed system were mounted on the same thrust balance used with tests in the 6' x 6' chamber. Figure 1 shows the thrust balance and Fig. 2 shows the balance, thrustor and feed system mounted in the 6' x 6' chamber. The installation in the 5' x 12' chamber was similar to that shown by Fig. 2.

The thrustor tested at high vacuum was identical to the one endurance-tested for 10 hours as reported in Ref. 4. In the 5' x 12' chamber the thrustor was operated at the same current and at about the same mass-flow-rate used in the life test. The thrust and voltage were close to those measured during the endurance test in the Arc Jet 6' x 6' chamber at 6×10^{-3} torr.

Table I lists the results from both the high-vacuum tests and the previous tests at higher pressures. Although the thrust

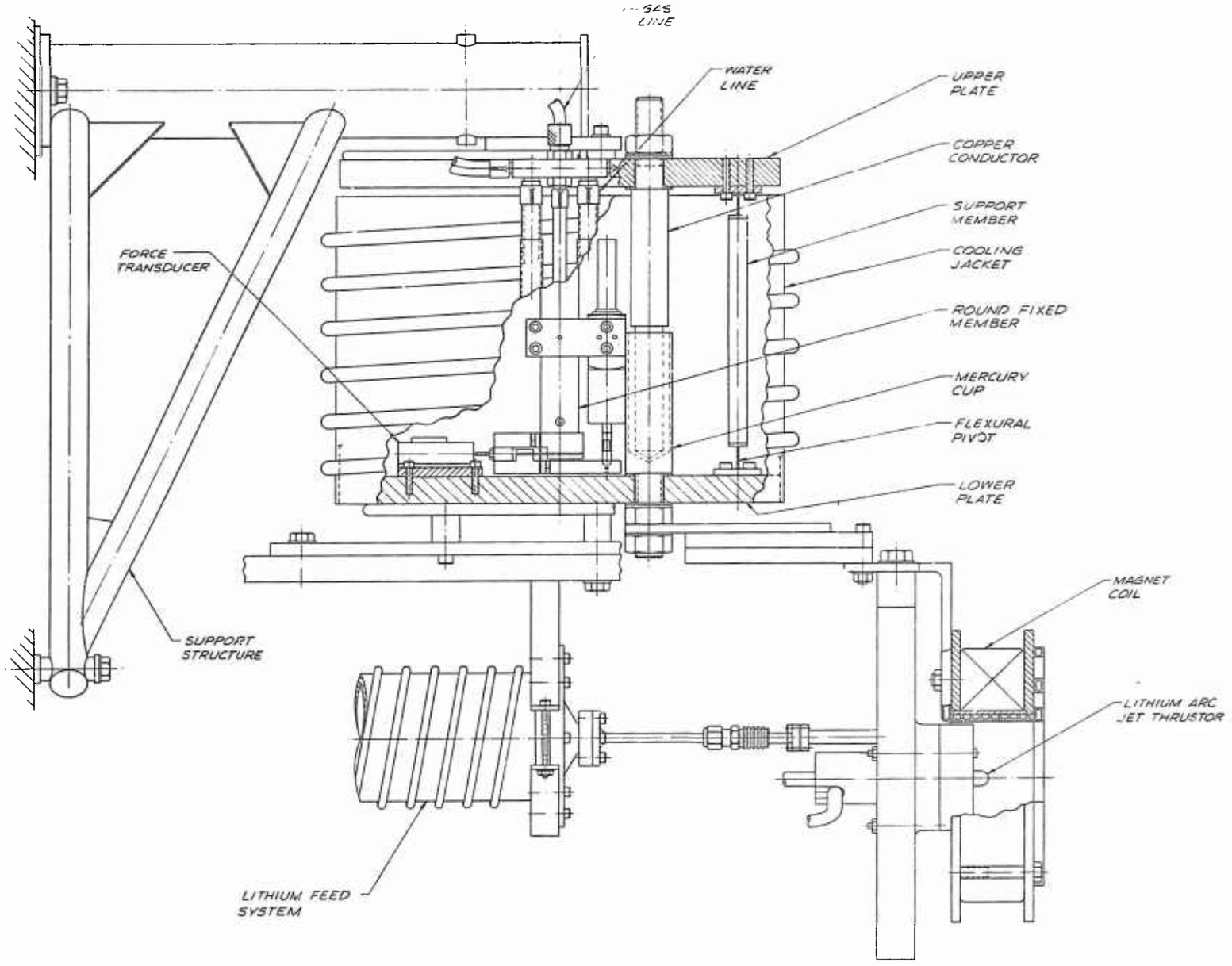

FIG. 1 LITHIUM ARC JET AND BALANCE ASSEMBLY

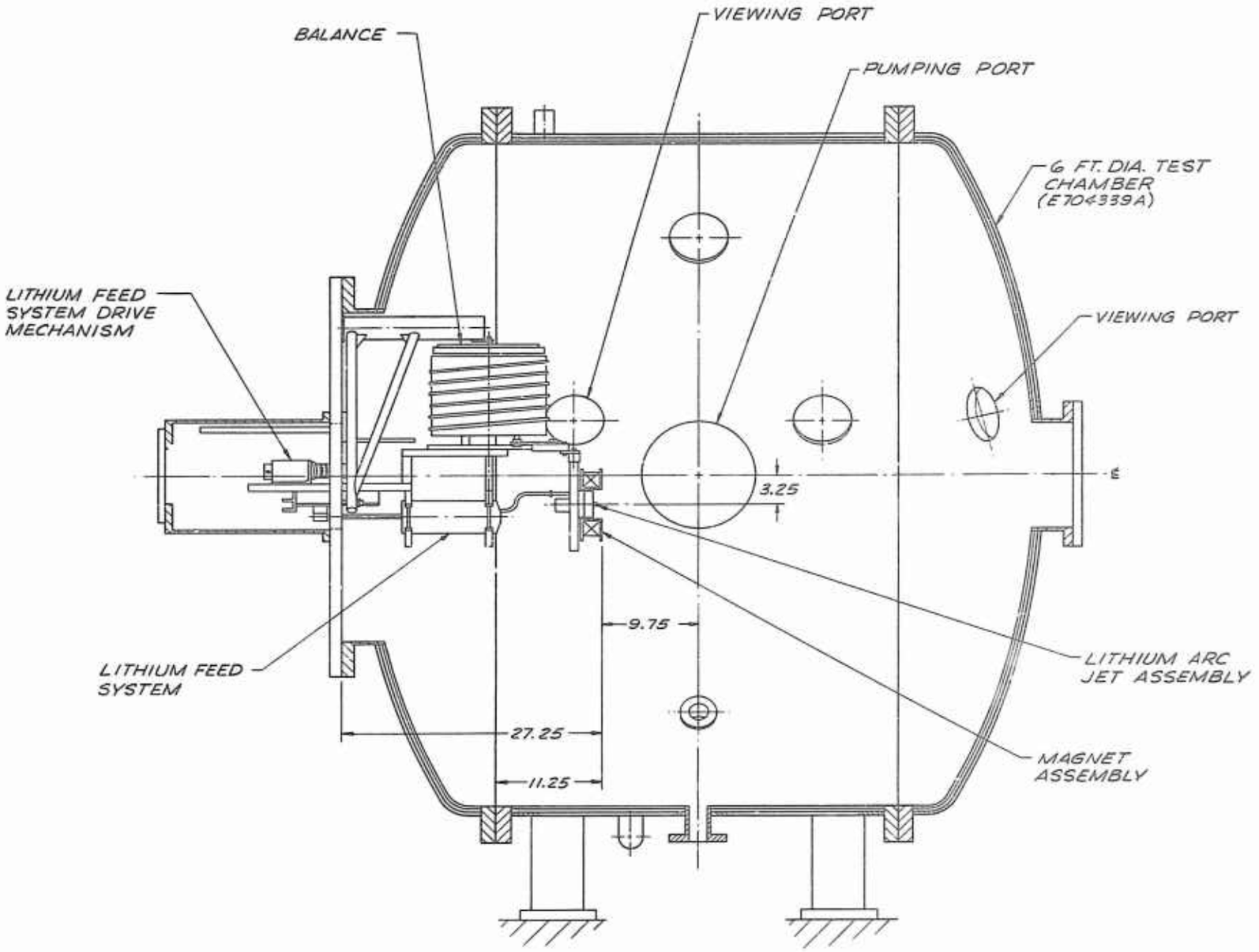

FIG. 2 LITHIUM ARC JET 6-FT-DIAMETER TEST CHAMBER

TABLE I

HIGH VACUUM TEST RESULTS

Arc Current (amps)	Arc Voltage (volts)	Power Input (kw)	Coil Current (amps)	Thrust (grams)	Mass Flow Rate (grams/sec)	I_{sp} (sec)	Efficiency	Tank Pressure (mm-Hg)
250	40	10.0	1800	22.5	0.0053	4950	0.53	6×10^{-3}
250	42	10.5	1800	24.4	0.0054	4540	0.51	2×10^{-7}
250	40	10.0	1800	22.8	0.0058	4040	0.44	3×10^{-7}
250	42	10.5	1800	23.8	0.0058	4110	0.45	2×10^{-7}

level in the high-vacuum tests was about the same as in the higher pressure test, the efficiency was slightly lower due to the higher mass-flow-rates.

The high-vacuum test was stopped when the arc attached to the condenser baffle-plates connected to the liquid-nitrogen-cooled liner adjacent to the wall of the tank. This attachment was caused apparently by the buildup of lithium condensed on the baffles. The baffles were removed and additional tests were attempted; however, the power density to the liner was then excessive and the liquid nitrogen in the liner boiled. As a result the test chamber pressure fluctuated over a large range. The test was stopped because of the danger of over-pressurizing the liner due to liquid nitrogen boiling. Any further testing of the arc jets in the 5' x 12' chamber will have to be at low power levels (below 2-3 kw) or it will be necessary to modify the liner or install a different type of condensing-baffle configuration.

From these test results and the pressure-effect testing previously reported in Ref. 7 it might be concluded that the thrustor performance may not be sensitive to pressure for pressures below the range of 10^{-2} to 10^{-3} torr. These results, however, must be viewed with some caution. The predominant effect of tank pressure is probably due to the entrainment of ambient tank gas into the plasma acceleration region, which is principally downstream of the engine. Indeed, it has been demonstrated that this type of thrustor will produce about the same thrust with hydrogen propellant injected through the tank walls as with injection through the thrustor. The present results, indicating no effect of pressure level on thrust, may be misleading. The possibility exists that the size of the interaction region increases as the pressure is decreased so that the mass entrainment rate does not decrease significantly with pressure. This does not appear to be the case from visual observations of the jet structure while the pressure is lowered; however, it still may be so.

It appears that the question of entrainment could be resolved by measuring the extent of the interaction region at various pressure levels. This could be done by determining the axial current distribution, as described in Ref. 8, by measuring the induced azimuthal magnetic field with a magnetic-field probe.

3.2 Measurement of Performance with Potassium

Potassium was investigated as a propellant in the Hall arc jet because of its potentially higher frozen-flow efficiency. Assuming the predominant energy loss to be ionization and further that all propellant atoms are ionized only once, the propellant with lowest loss and highest efficiency is the one with the lowest first ionization potential per atomic mass unit. Among the alkali metals this ratio, V_I/m_a, decreases for increasing atomic weight. On the other hand as the atomic weight increases the second ionization potential V_{II}, decreases, the kinetic energy for a given specific impulse increases, and the number density of the plasma decreases for the same power density and specific impulse. Therefore, second ionization and energy losses (in addition to first ionization) are more likely to occur as the atomic weight increases. Since it is not possible at this stage to evaluate these effects and calculate the efficiencies on the basis of experimental results with other propellants, the potassium experiments were carried out.

The experimental results were quite different from predictions based on first-ionization energy losses. The efficiency was lower than with lithium at the same specific impulse and the maximum specific impulse attainable was only 1500 sec compared to 6000 to 8000 sec with lithium.

To eliminate geometry effects from the comparison of lithium and potassium, the same thrustor configuration (Model LAJ-AF-6D, Fig. 3) was used with both propellants. This certainly eliminated one form of ambiguity in the results but may have created another. The configuration used was to some extent optimized for lithium. It is possible

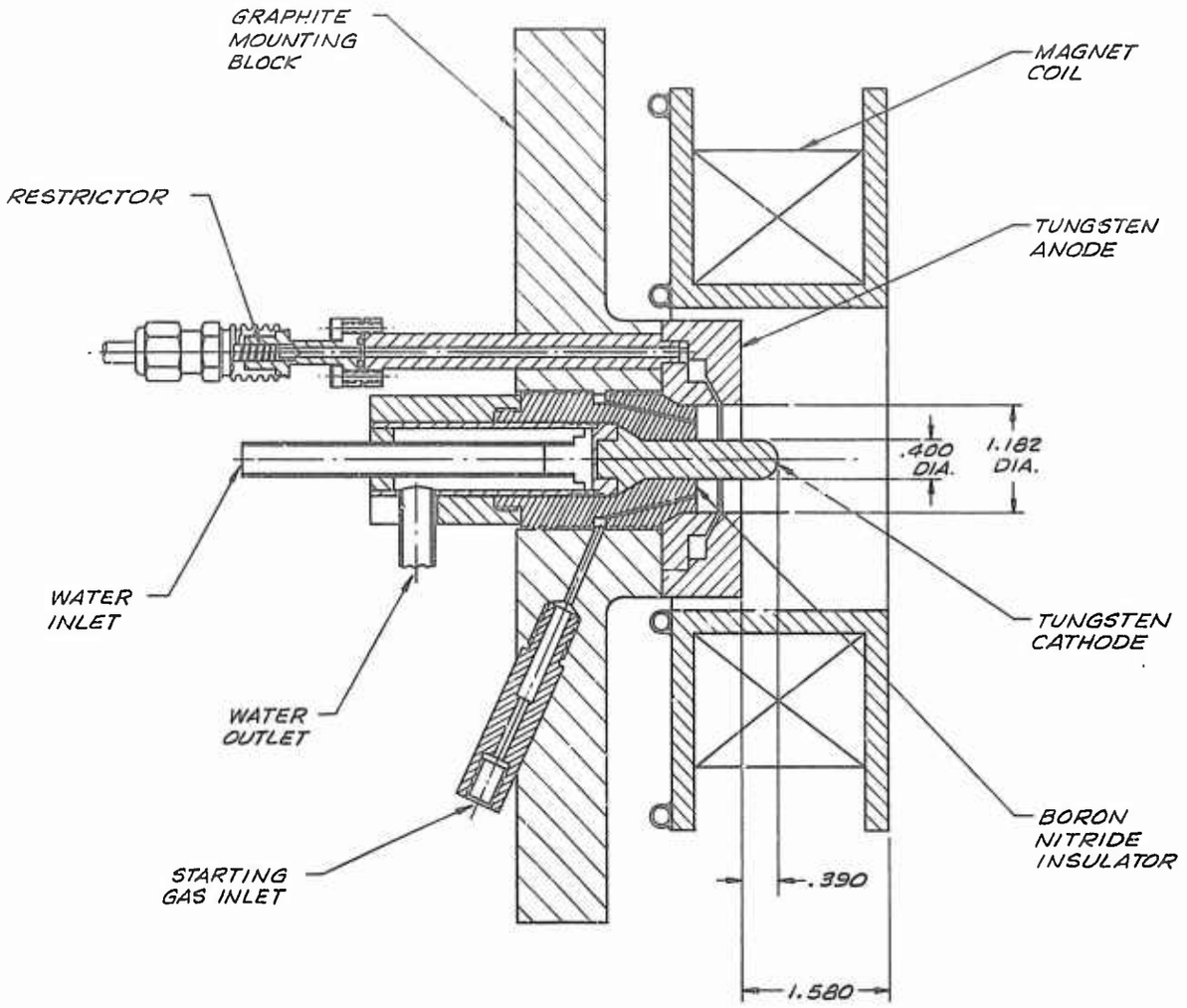

FIG. 3 ARC JET MODEL LAJ-AF-6D

that through a systematic variation of thrustor geometric parameters using potassium, improvements in performance could be found. In other words a thrustor optimized for potassium should be compared with the lithium thrustor. The principal geometric variable of concern is the jet diameter, which directly affects the number density of the plasma in the acceleration region. This points out the need for additional fundamental understanding and analytic parameters to describe the effects of geometry and propellant properties on the thrustor performance.

Although the studies of potassium performance did not include variations of geometric parameters, the effects of the magnetic field strength, arc current, and test chamber pressure on thrust, total arc voltage, tank floating voltage, and anode power loss, were measured.

As Fig. 4 shows, the specific impulse was varied over the range of about 600 to 1600 sec. The corresponding thrust efficiency varied from about 12 percent to 28 percent. Note that the thrust efficiency increases with specific impulse when the specific impulse is less than about 1200 sec, but does not appear to increase between 1200 and 1700 seconds. This asymptotic or peaking tendency of the thrust efficiency may be an indication of the beginning of second ionization. This maximum specific impulse is related to the tendency of the thrust to decrease as the mass-flow-rate is decreased at constant arc current.

The results of Fig. 4 were measured in a chamber-pressure range ($2 - 8 \times 10^{-4}$ torr) where it appears that the thrust may be independent of pressure level. Figure 5 shows thrust as a function of chamber pressure over a range from 10^{-4} to 10^{-1} torr. These results are only approximate because they were obtained in a transient condition during which the pressure was first increasing and then decreasing. The pressure was varied by bleeding argon into the

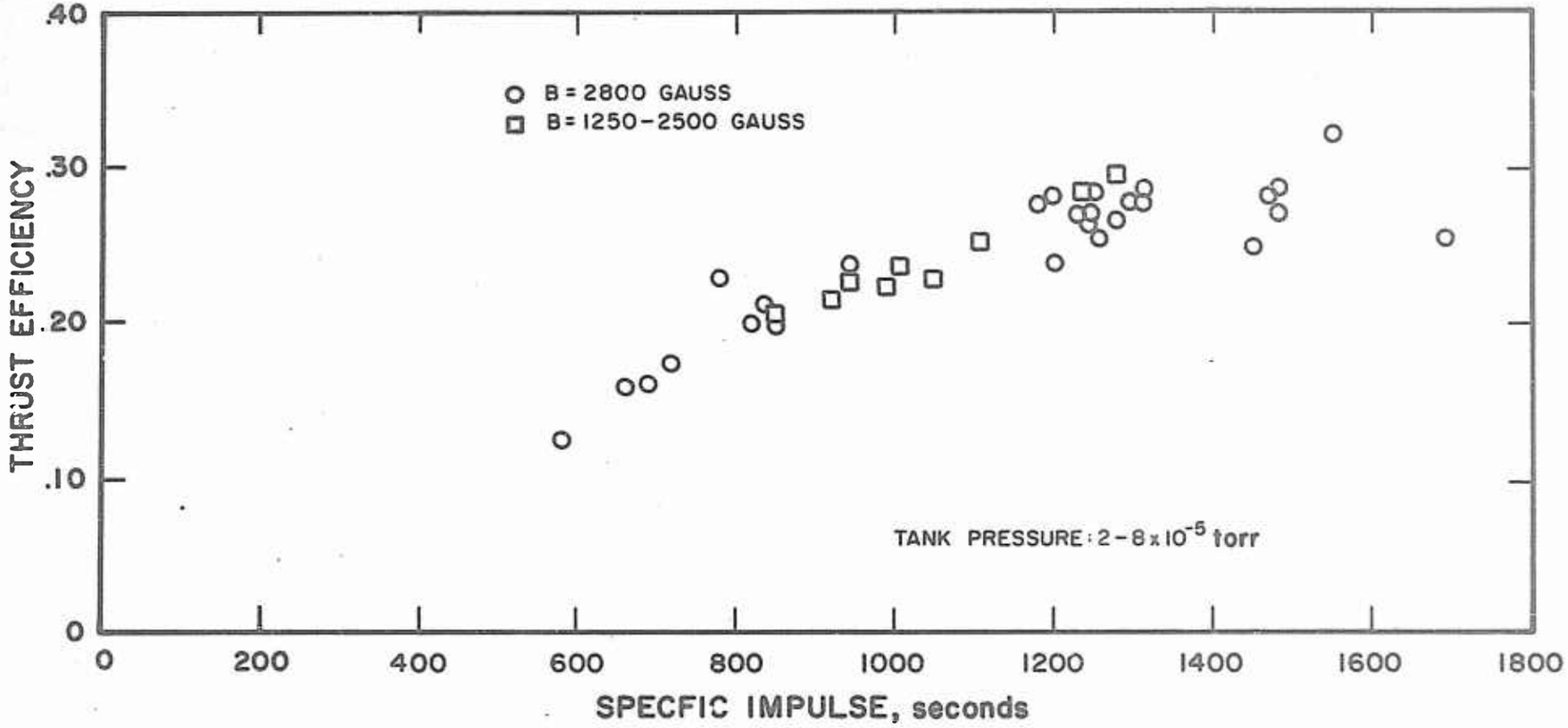

FIG. 4 HALL ARC JET PERFORMANCE WITH POTASSIUM

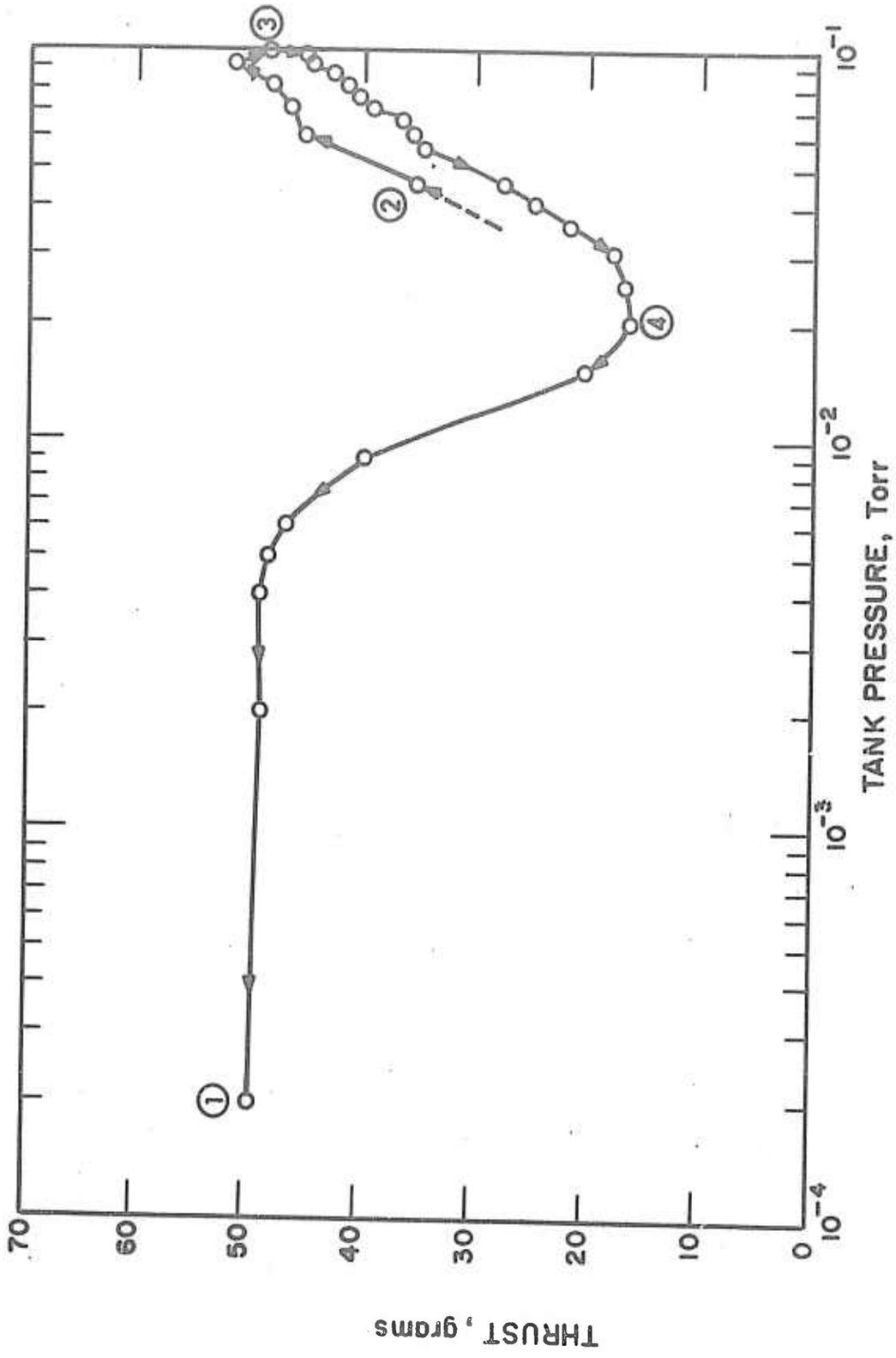

FIG. 5 THRUST VS TANK PRESSURE WITH POTASSIUM

chamber. The sequence was begun at the point indicated by (1) on Fig. 5. The pressure rapidly rose and the thrust decreased to some minimum value and then increased. Beginning at point (2) (Fig. 5) pressure was recorded as a function of thrust. The pressure rose to 10^{-1} torr (at point (3)) and then began to drop. The thrust was maximum roughly at the maximum pressure and then dropped as the pressure decreased. The thrust reached a minimum at about 2×10^{-2} torr (point (4)) and then increased to an apparent asymptotic level at about 4×10^{-3} torr. (Pressures above 10^{-3} torr were measured with a thermocouple type vacuum-gage and below 10^{-3} torr with an ionization gage.)

It appears that the region to the right of the asymptotic level of pressure is the region where a significant rate of ambient gas is entrained into the thrusting region of the discharge. The asymptotic level probably varies with the thrustor operating conditions, and should be investigated further.

The effects of magnetic field strength on thrust and voltage are shown in Fig. 6. The thrust increased with increasing magnetic field for field strength up to about 2500 gauss. Above 2500 gauss the behavior is not clear because of insufficient data; however, it appears that the thrust may be independent of field strength, or may reach a maximum and then decrease with increasing field strength. This tendency may also be due to the onset of second ionization. As Fig. 6 shows, the total arc voltage increased with increasing magnetic field strength from about 24 volts at 1200 gauss to about 40 volts at 2800 gauss.

Figure 7 shows the effect of the magnetic field strength on the voltages measured between the anode and the tank and between the tank and the cathode. Similar measurements with sodium* as the propellant are shown for comparison. As Fig. 7 shows, the anode-to-tank

*Sodium measurements were made on NASA Contract NAS3-5909

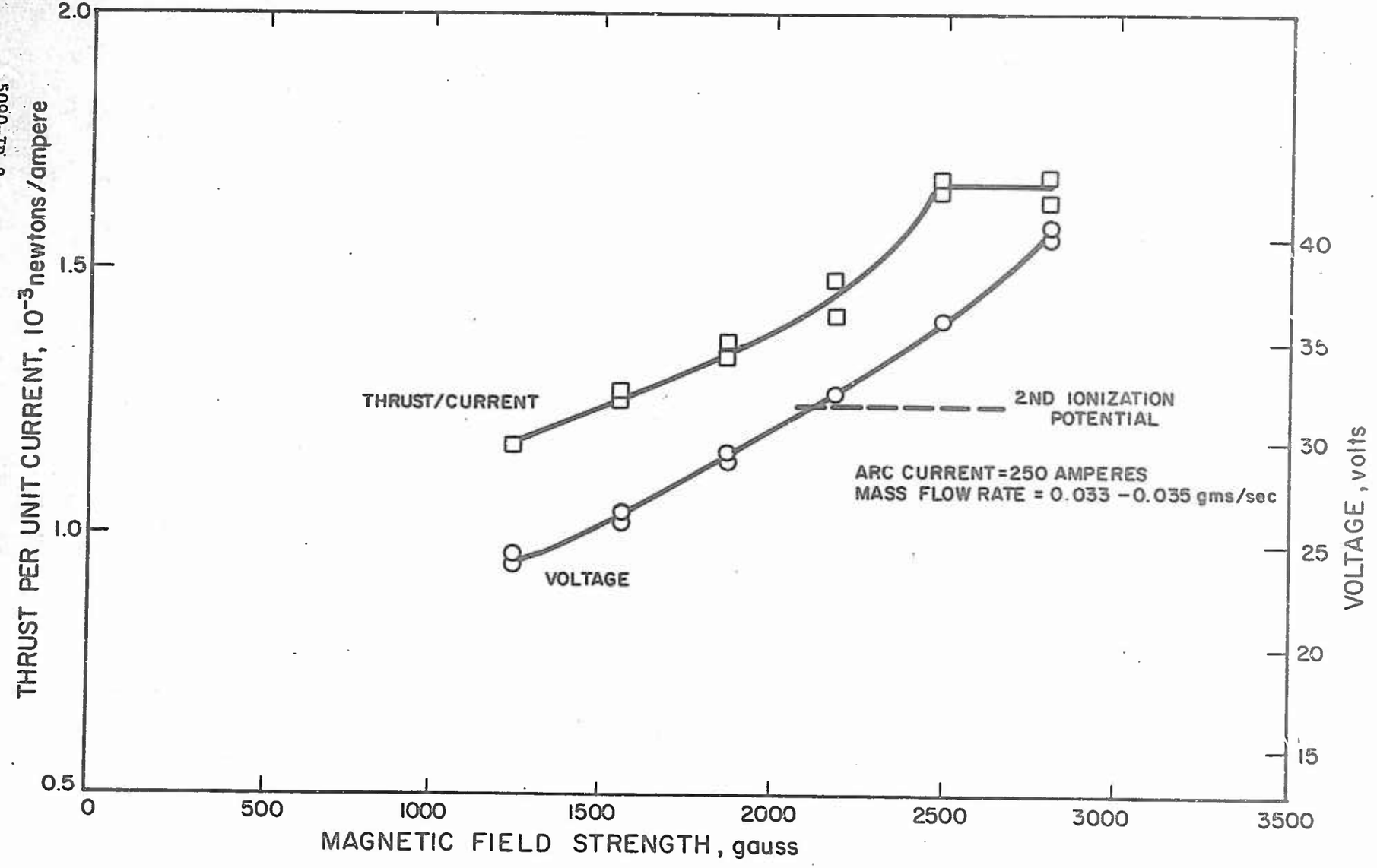

FIG. 6 EFFECT OF MAGNETIC FIELD STRENGTH ON THRUST AND VOLTAGE FOR POTASSIUM

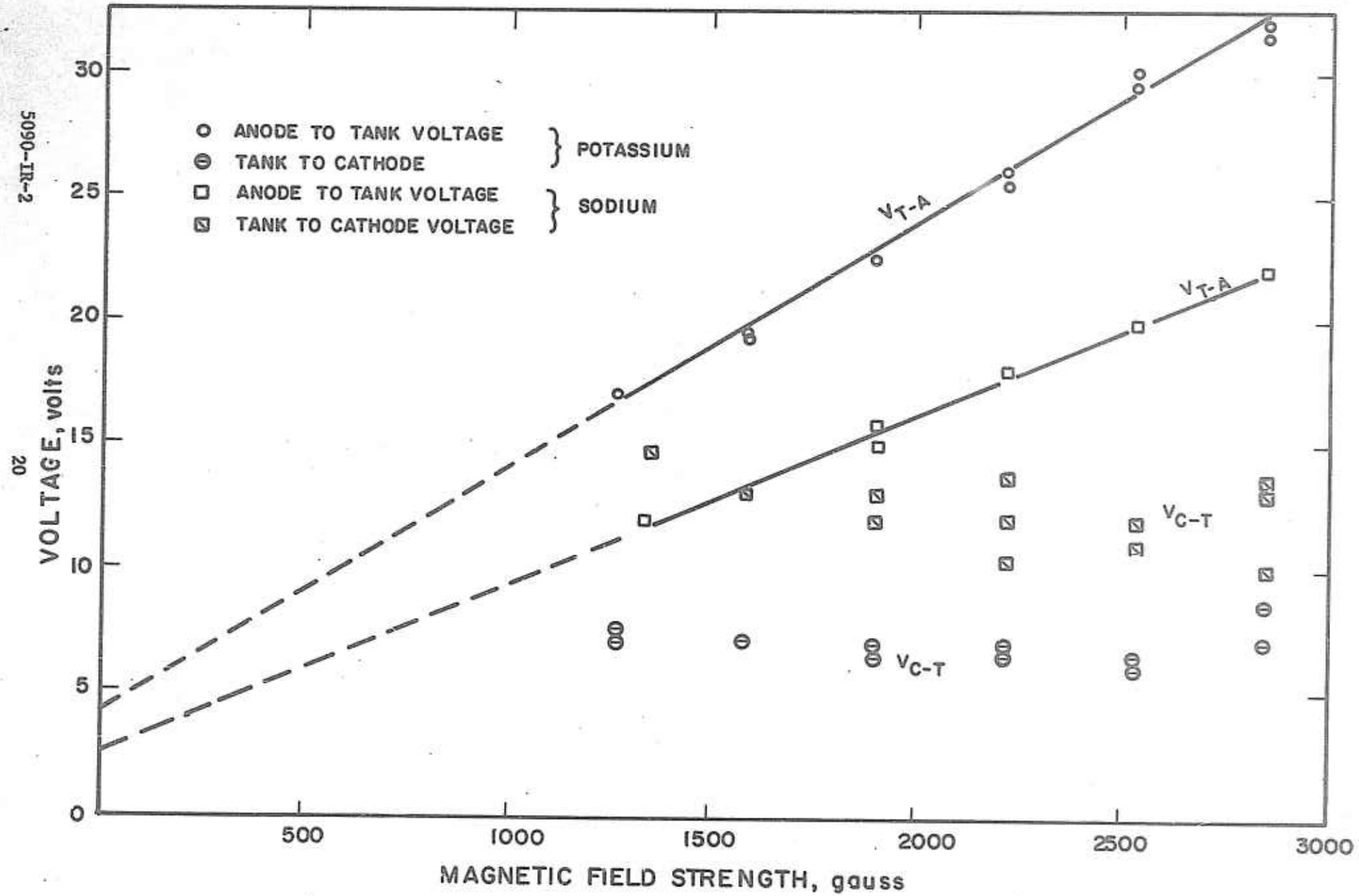

FIG. 7 EFFECT OF MAGNETIC FIELD ON ARC POTENTIALS FOR SODIUM AND POTASSIUM

voltage increases with magnetic field strength while the tank-to-cathode voltage appears to be independent of the magnetic field. Since the tank floats near the cathode potential or at least near the potential of the cathode jet, this observed result seems to indicate that the conductivity along the cathode jet is independent of the magnetic-field strength.

Figure 8 shows a correlation of the power loss to the anode for both potassium and sodium.* Note that the anode power loss divided by the arc current has the same value for sodium and potassium when the straight lines through the data are extrapolated to zero field strength. Also, the slopes for potassium and sodium differ in magnitude approximately by the inverse of the square of their molecular weights. This may be a coincidental rather than a universal relationship since the mass-flow-rate, arc current, and Ψ values were different for the two propellants. Power loss to the cathode as a function of the arc current is shown in Fig. 9. The power loss depends primarily on the arc current and as the data show it is relatively insensitive to the mass-flow-rate and magnetic field strength. The average power loss divided by the arc current (apparent cathode voltage drop) is about 5 volts.

Thrust varies about linearly with arc current as Fig. 10 shows. The maximum current during these runs was 400 amperes at which point the cathode-anode insulator and the cathode began to erode. Figure 11 shows the thrust per unit current and total arc voltage for potassium plotted as a function of the parameter $\Psi = \frac{|e|\dot{m}}{m_a I}$. This parameter seems to correlate the data reasonably well. A region ($\Psi > 0.35$) is indicated where the thrust per unit current is independent of Ψ. In the region where $\Psi < 0.35$ the thrust

*Sodium measurements were made on NASA Contract NAS3-5909

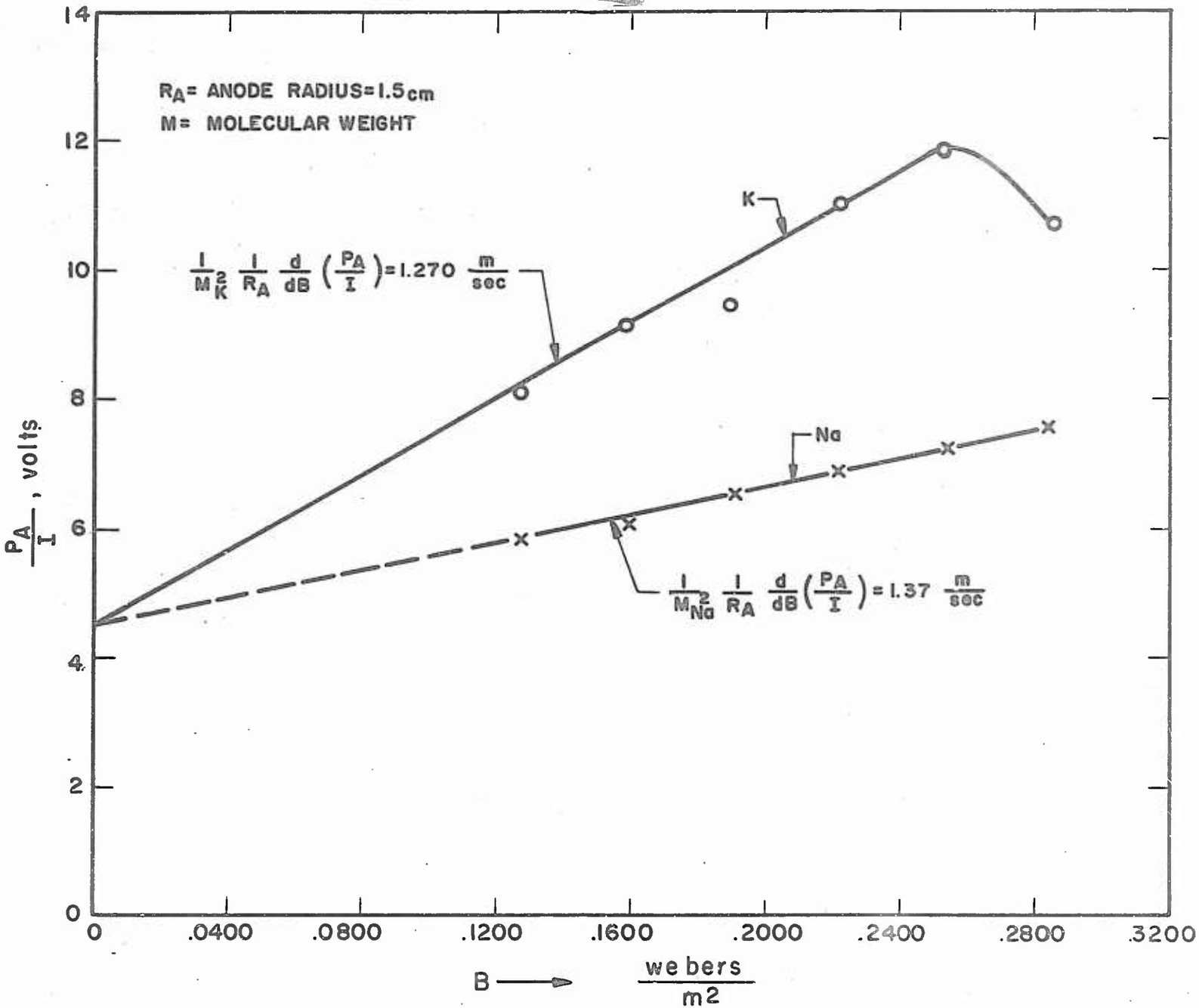

FIG. 8 EFFECT OF MAGNETIC FIELD STRENGTH ON ANODE POWER LOSS FOR SODIUM AND POTASSIUM

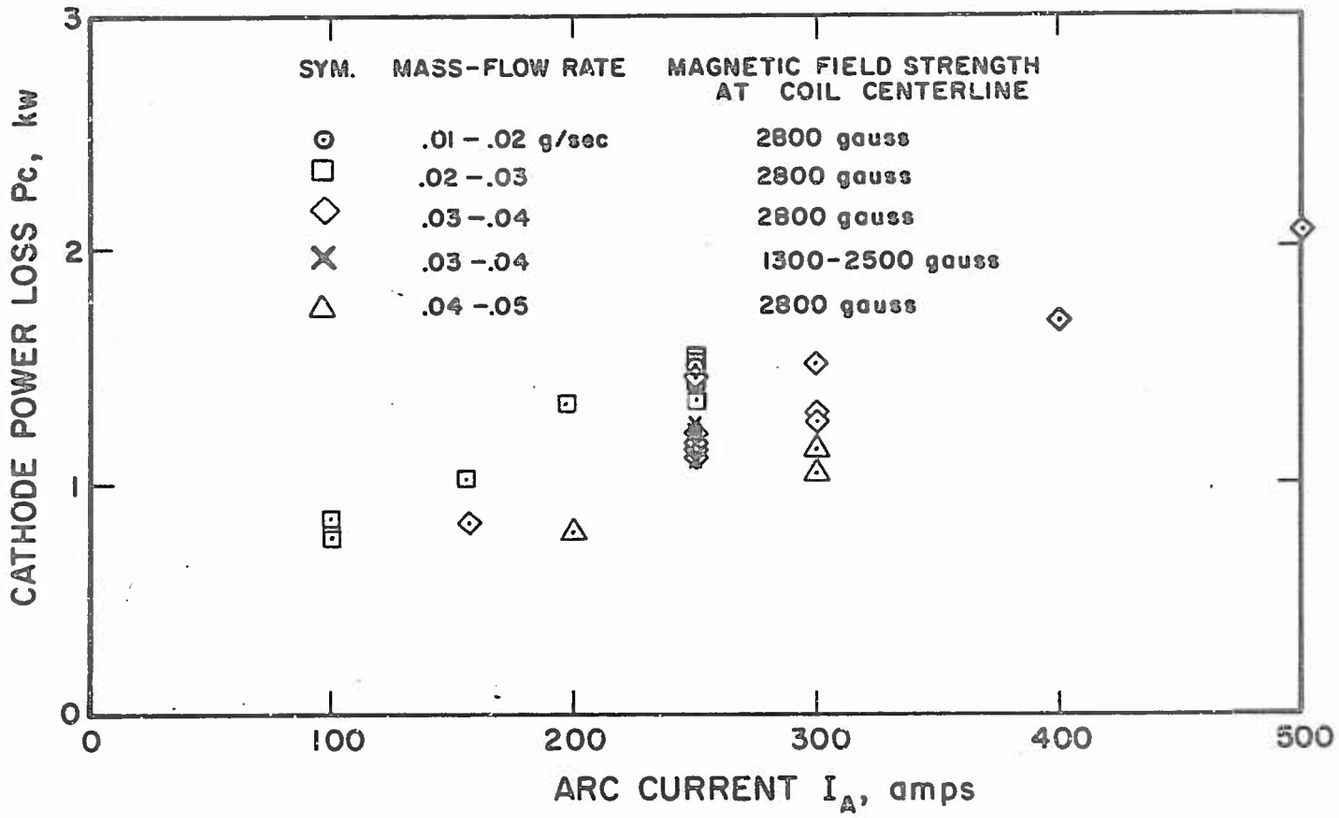

FIG. 9 CATHODE POWER LOSS AS A FUNCTION OF ARC CURRENT

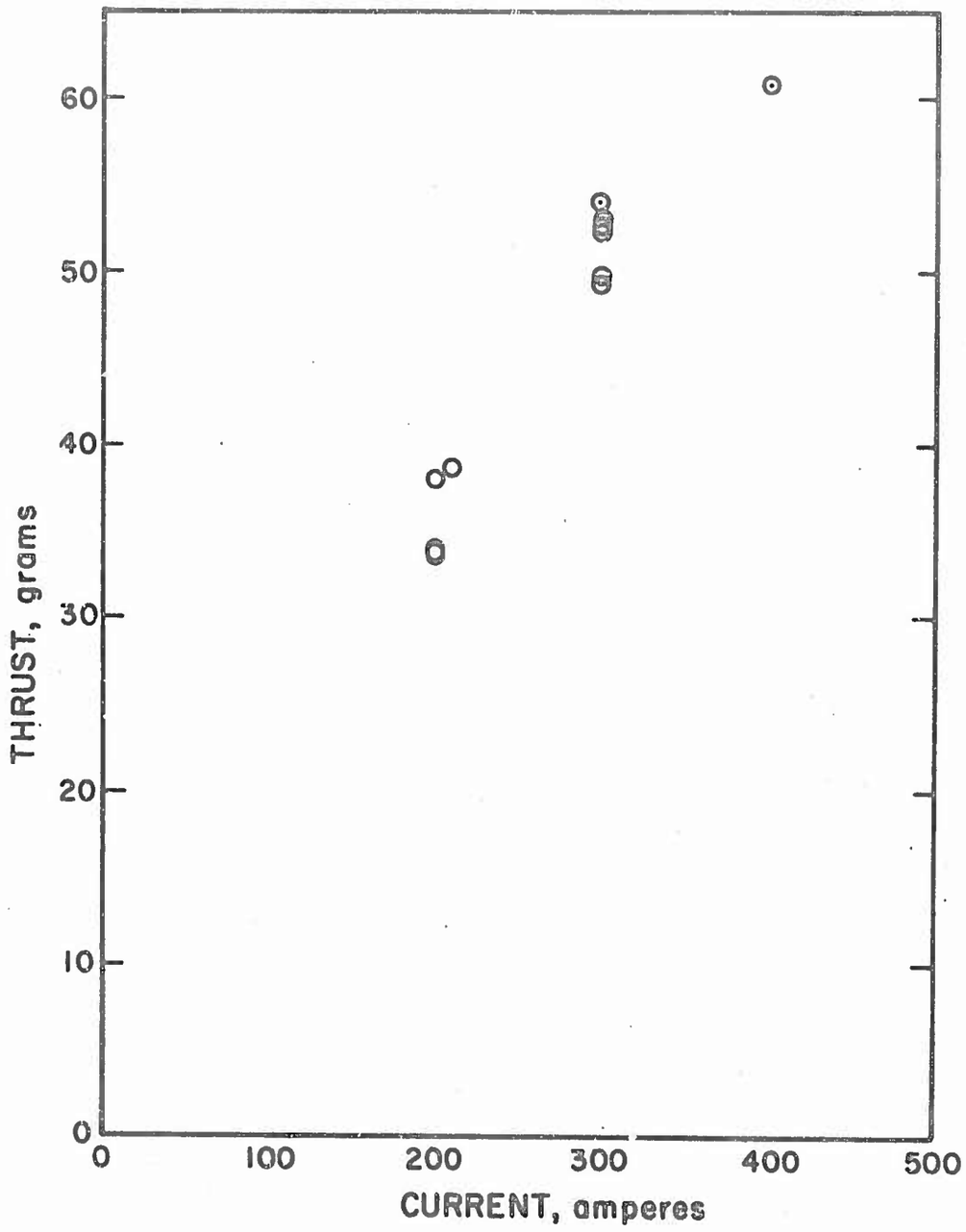

FIG. 10 THRUST VERSUS CURRENT WITH POTASSIUM

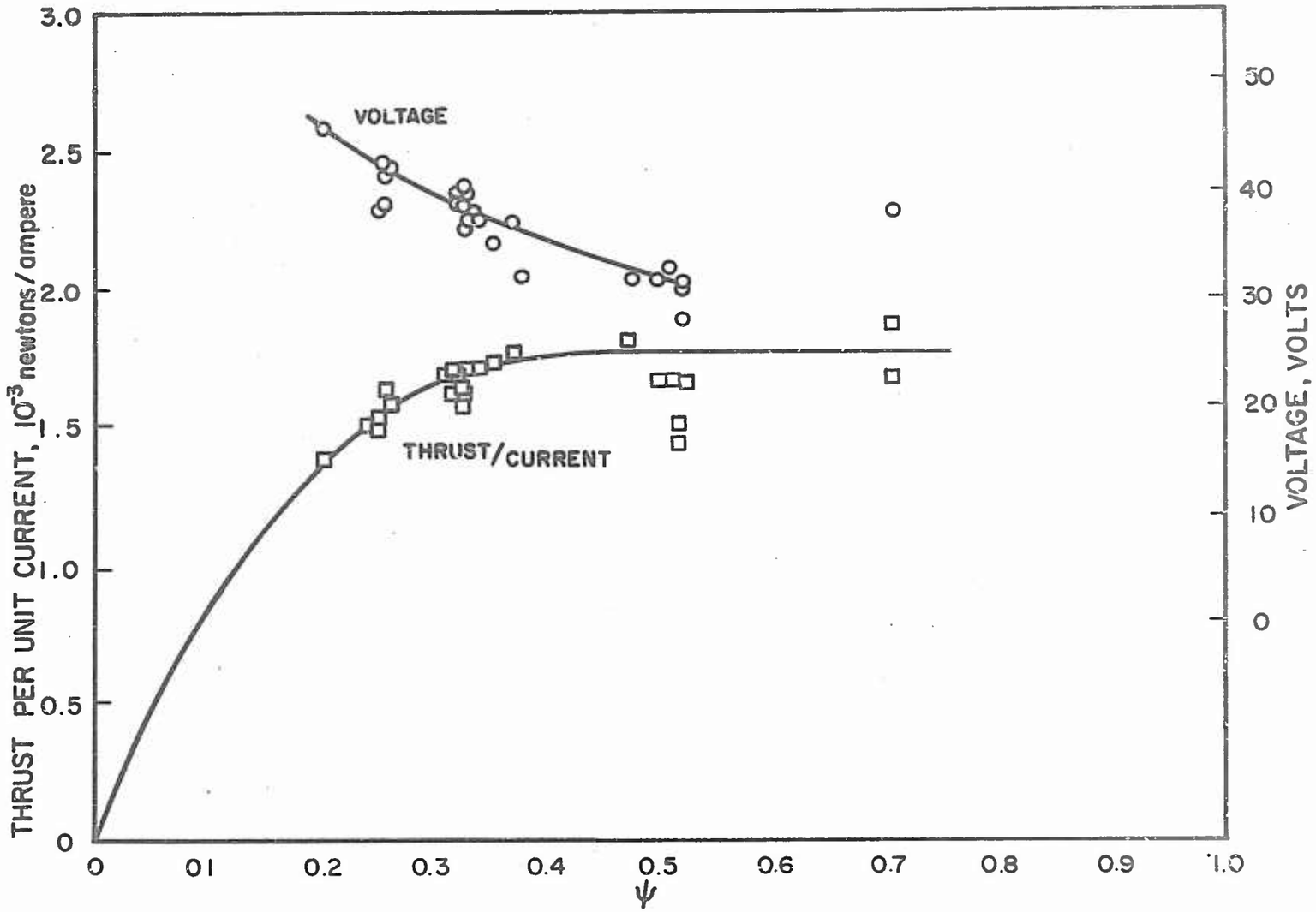

FIG. 11 THRUST PER UNIT CURRENT, VOLTAGE AS FUNCTION OF PARAMETER, $\Psi = \frac{|e|}{m_a}\frac{\dot{m}}{I}$, FOR POTASSIUM

per unit current decreases with decreasing Ψ, i.e., with decreasing mass-flow-rate or increasing current. The arc voltage decreases with increasing Ψ as the analysis of Ref. 4 predicts.

For the potassium experiments the thrustor and feed system were mounted directly on a thrust balance (described in detail in Ref. 4) and installed in the 6' x 6' test chamber. The scheme was identical to that used in the lithium experiments as described previously (see Figs. 1 and 2). The variables measured were thrust, mass-flow-rate, arc current and voltage, magnet coil current and voltage, test chamber pressure, and heat transfer to the coil, cathode, anode, and test chamber.

Since the anode was radiation-cooled it was necessary to use an oil-cooled shield to absorb the radiation from the anode radiation fin. This shield intercepts only the radiation from the rear (upstream) surface of the fin. Radiation from the front surface of fin, from the outside cylindrical surface of the anode, and most of the radiation from the front surface of the anode itself is absorbed by the magnet coil housing. The sum of the powers transferred to these oil-cooled components is approximately equal to the anode power loss. Power transfer was determined by measuring the cooling-oil flow rate and temperature rise.

The potassium was fed into the thrustor with the bellows feed system developed for lithium. This feed system is described in detail in Ref. 4. A recent calibration of the feed system accomplished during the reporting period is presented in Section 5.

3.2.1 Spectrographic Analysis of Plasma Radiation from Potassium Thrustors

The optical energy radiated by potassium thrustors was recorded spectrographically in the 2800 to 6500Å range. The potassium plasma was viewed from the side, so that a cylindrical disk of the plasma (perpendicular to the plasma axis, and 1/2 to

5 inches downstream of the anode) was imaged on the spectrograph slit. A 1.8-meter quartz Littrow-type spectrograph provided both a spatially and a spectrally-resolved image on the photographic plate.

The radiation was most intense from a bright cylindrical core along the axis of the engine. Only ionized species of potassium (KII) and contaminants are observed in this core -- no atomic or molecular species are detected. The radiation intensity appears to be greatest on the core surface, indicating a large ion density in the core, or a high excitation temperature caused by electrons trapped in the thrustor magnetic field lines.

The intensity of the ion lines is sharply lower outside the core, and decreases rapidly for larger radii. Atomic and molecular species also radiate outside the core, although the strong potassium atom (KI) lines at 4044.14 and 4047.20Å are weaker than many of the potassium ion lines (KII) in this portion of the spectrum.

The spectral lines were tabulated to determine if doubly-ionized species were observed in the plasma. Nearly all lines on the spectrographic plates were accounted for by singly-ionized and atomic potassium (KI and KII), and ionic and molecular contaminants. No multiple ionized species could be detected.

Contaminants in the central core included ionized calcium (CaII) and boron (BII), both apparently originating from the boron nitride insulator used in the thrustor. Emission outside the core includes molecular bands due to ionized molecular nitrogen (N_2^+), molecular nitrogen (N_2), and possibly molecular NH. The intensity of these bands, relative to the intensity of the potassium spectrum, varied with operating conditions and for tests with different thrustors. These contaminants are easily detected by spectrographic analysis (detectability about 0.1 parts per million by weight) and may represent extremely small plasma contamination.

3.3 Future Thrustor Tests

It is presently planned to measure the performance characteristics of:

1. A thrustor with a buffered cathode configuration.
2. A high-power (100 kw) thrustor, and
3. A low-power (1 kw or less) thrustor.

The objective of the buffered-cathode configuration shown in Fig. 12 is to operate the cathode in a spot-attachment mode. Experience has indicated that with gases the attachment mode is determined primarily by the pressure level although the geometry and flow pattern around the cathode are also significant parameters. In the cathode study reported in Ref. 9 the stable spot-attachment mode prevailed at pressure levels above about 1 psia. In this mode the apparent cathode voltage drop (defined as power loss divided by arc current) was only about one volt and the cathode erosion rate was negligible. At pressure levels below about 1 psia, the cathode attachment became more diffuse, was unstable, the apparent voltage drop increased to several volts, and the erosion became severe. In the alkali-metal arc jets described here and in Ref. 4, the pressure at the cathode has been very low (not measured but estimated to be in the order of 10 torr). The attachment mode was diffuse and in some cases unstable. The apparent cathode voltage drop has been about 5 volts and the erosion rate has been greater than desired. It is the intent in the buffered-cathode design to increase the pressure level at the cathode to decrease the power loss and erosion.

Referring to the details of the thrustor design (Fig. 12), the propellant vapor will be injected through the annular slot of the buffer upstream of the cathode tip and the buffer throat, which is 0.10 inches in diameter. With a propellant flow rate of 1 - 2 x 10^{-3} gm/sec it is estimated that the pressure at the cathode tip will be of the order of 0.1 atmospheres. This pressure should be sufficiently high for the arc to attach in a small spot at the tip of the conical cathode.

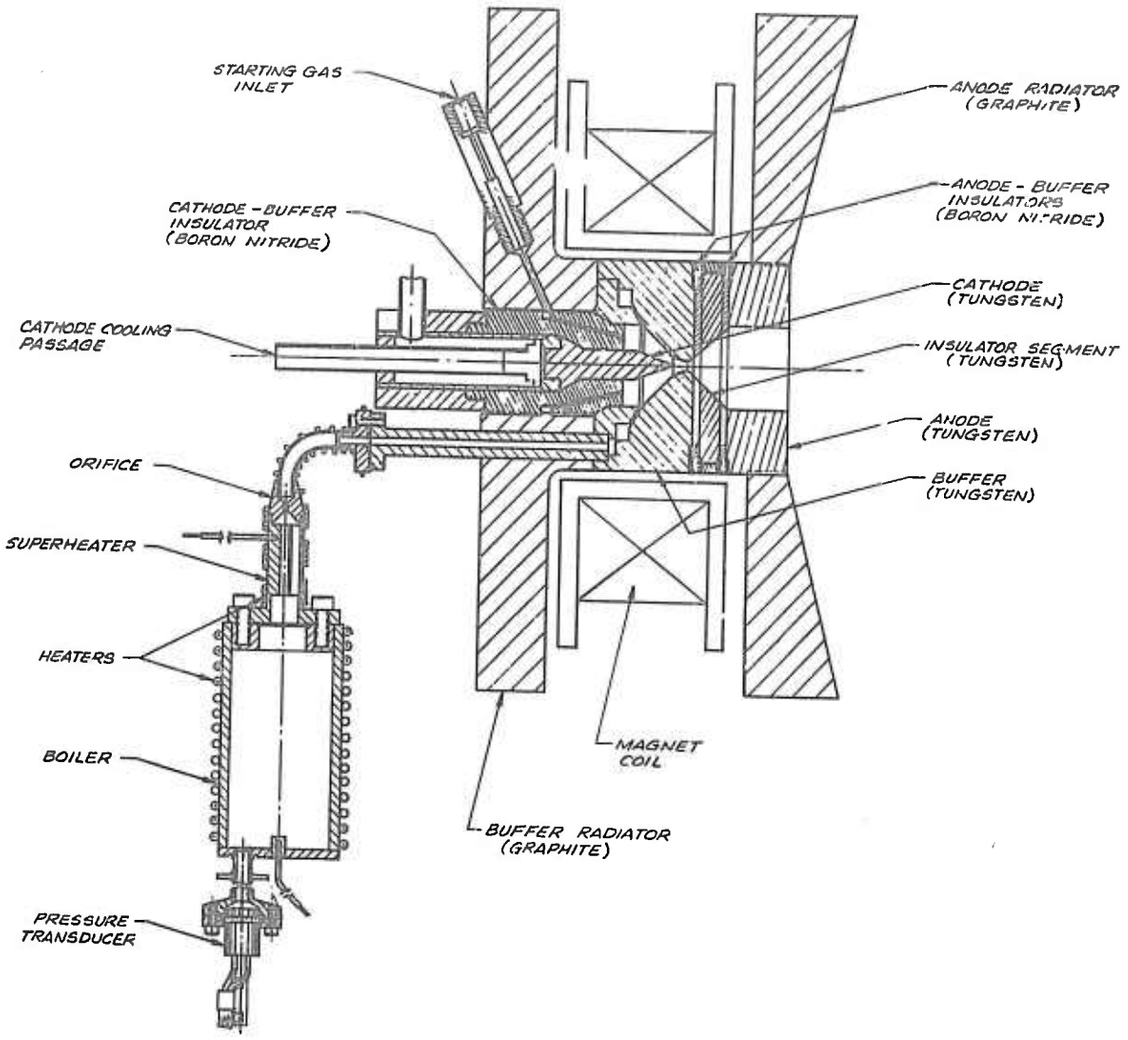

FIG. 12 BUFFERED-CATHODE THRUSTOR CONFIGURATION (Model LAJ-BF-1)

This thrustor is radiation-cooled with the exception of the water-cooled cathode. Graphite disks attached to the buffer and the anode enhance the radiation-cooling capacity. Note that much of the radiation will be absorbed by the water-cooled magnet-coil housing. In addition there will be a water-cooled shield (not shown in Fig. 12) behind the buffer radiator. The total power lost to the buffer will be determined by measuring the power absorbed by the shield and the inner and rear portions of the magnet-coil housing.

4. ANALYTICAL STUDIES

4.1 Acceleration Mechanisms

The ability of axisymmetric Hall current plasma accelerators to produce significant amounts of thrust has definitely been established. However, the mechanisms by which the propellant is accelerated are still not completely understood, making it difficult to design optimum engines. Some general considerations of this problem are discussed below and one mechanism is identified as that most likely responsible for the axial acceleration of the gas, which results in the production of thrust.

A few general rules that are of value in guiding the discussion are listed below:

1. Thrust is produced only by the expulsion of high-velocity particles from the thrustor. In electromagnetic devices these particles must be predominantly ions, accompanied, of course, by an equal number of electrons, moving at the same exhaust velocity. Because of their low mass, the electrons do not make any significant contribution to the momentum of the exhaust beam.
2. The ions can attain high axial velocities through the following mechanisms:
   a. Conversion of ion enthalpy into kinetic energy by expansion through a mechanical or a magnetic nozzle.
   b. The conversion of ion azimuthal energy into axial kinetic energy by expanding the rotating plasma through a magnetic nozzle.
   c. Acceleration of the ions through an applied axial potential when either radial or tangential magnetic fields are present.

d. Acceleration of the ions through an axial potential drop which is supported by an electron pressure gradient. Except for elastic collisions, this is the only mechanism through which electron energy can be transferred to the ions and is, by far, the most effective at low number densities.

3. When an electric discharge occurs such that the current flows along axial magnetic field lines, no momentum in the axial direction is transferred between the plasma and the electromagnetic field. The energy dissipated in such a discharge is all transferred originally into the internal energy of the electrons.

4. In the discharge region ions are produced by inelastic collisions of atoms and electrons. The electrons gain the energy necessary to ionize the gas by carrying some fraction of the discharge current.

In discussing the thrust-producing mechanisms, it is convenient to divide the discharge into two regions, the cathode jet* and the anode sheath*. Little loss of generality occurs by assuming that the discharge occurs in a uniform axial magnetic field. In practice, the applied magnetic field will diverge.

It has been observed that the outline of the cathode jet tends to follow magnetic field lines, hence we shall assume that the cathode jet is a constant area discharge along the axis of the engine. The only thrust produced in the cathode jet is that due to the confining force of the self-magnetic field creating a pressure which reacts on the cathode to produce thrust. The gas in the cathode

*The cathode jet and anode sheath are those regions of the discharge emanating from the electrodes and following the direction of the magnetic field. These distinct current-carrying regions are visible and their existence has been verified by measurement of the axial current distribution across and along the discharge (Ref. 8).

jet is heated and exhausted sonically out of the confining cylinder produced by the self-magnetic field. The thrust obtained from this gas is:

$$T = \frac{\mu_o I^2}{8\pi} = \dot{m}_c \sqrt{\frac{2 \gamma k T_c}{m_a}}$$

where

$\dot{m}_c$ = mass-flow-rate out of cathode jet

T_c = exit temperature of gas from cathode jet.

If no mass is entrained into the cathode jet, further relations can be obtained. The voltage drop along the jet is given by:

$$V = \frac{\gamma + 1}{\gamma - 1} \frac{1}{\Psi} \frac{|e|}{2 m_a} \left(\frac{\mu_o I}{8\pi}\right)^2 + \Psi V_I$$

If the gas in this cathode cylinder is expanded out through a magnetic nozzle, the thrust obtained from this gas can be increased by the factor $\sqrt{\frac{\gamma + 1}{\gamma - 1}}$. For a monatomic gas this is equal to 2. The maximum I_{sp} and efficiency obtainable from the gas in the cathode jet is as follows:

For the constant area cathode jet

$$T_{max} = \sqrt{\frac{\gamma + 1}{\gamma - 1}} \quad \frac{\mu_o I^2}{8\pi}$$

$$V = \Psi V_I + \frac{\gamma + 1}{\gamma - 1} \frac{1}{\Psi} \frac{|e|}{2 m_a} \left(\frac{\mu_o I}{8\pi}\right)^2$$

$$(I_{sp})_{max} = \frac{\mu_o I^2}{4\pi \dot{m}_c}$$

$$\eta_{max} = \frac{1}{1 + \frac{\gamma - 1}{\gamma + 1} \frac{2 m_a V_I}{|e|} \left(\frac{8\pi \Psi}{\mu_o I}\right)^2}$$

Although it is not evident from the above expression, half of the thrust shown above is due to the reaction on the magnet forming the magnetic nozzle.

The acceleration mechanisms in the anode jet can most conveniently be investigated by assuming that all of the mass in the anode jet leaves the anode through a thin annulus in the anode front face at a radius of R_{A_o}. We shall also assume that the gas is fully ionized as it leaves the anode. The analysis of the anode sheath indicates that it must decrease in diameter as it moves downstream. This results in an increase in the axial velocity due to the self-magnetic interaction and a spinning up of the gas due to the current crossing the magnetic field lines. Once the anode sheath meets the cathode jet the axial and rotational velocity are given by the following expressions:

axial:
$$w = \sqrt{2\gamma \frac{k T_a}{m_a} + \frac{\mu_o I^2}{4\pi}\left(\frac{1}{4} + \ln \frac{R_{A_o}}{R_{C_o}}\right)}$$

azimuthal:
$$v = \frac{B_o I}{2 \dot{m}_A} \frac{\left(R_{A_o}^2 - R_{C_o}^2\right)}{R_C}$$

The ions have obtained this axial velocity by acceleration through an axial electric field that has been established along the jet. The azimuthal velocity of the ions has been built up by:

1. Ion acceleration in a crossed radial electric field and axial magnetic field.
2. Collisions with the electrons which have azimuthal velocities higher than the ions, i.e., Hall currents are flowing. When the applied axial magnetic field strength is much larger than the induced azimuthal magnetic field it can be shown that:

$$|v| >> |w|$$

when

$$B_z >> \frac{\mu_o I}{2\pi R_c}$$

Because of the low density of the gas in the anode sheath it can also be shown that a negligible amount of the energy transferred out of the electric discharge is in the internal energy of the ions as they enter the cathode jet. This, then, indicates that for the gas in the anode sheath, the energy is originally almost all transferred into the rotational energy of the gas in the discharge region. As the gas then expands through the magnetic nozzle and conserves angular momentum, a large fraction of this energy can be converted into axial kinetic energy. If this is indeed the mechanism by which most of the thrust is produced by the engine, then some of the consequences would be:

1. When some of the current in the anode sheath is carried by electrons the ions will be spun up to velocities such that

$$\frac{1}{2} m_a v^2 > |e| V_A$$

where V_A is the potential drop which occurs along the anode sheath. This then gives a logical and believable mechanism by which the gas exhaust energy per particle can be greater than would be obtained by falling through the arc potential drop.

2. The propellant should be injected through the anode.
3. The propellant should be ionized as near the anode as is possible, preferably inside of the anode.

At this point in the discussion it is of value to ask what role the Hall currents play in the acceleration mechanism postulated above. First, the azimuthal electron drift which comprises the Hall

currents occurs because of the poor mobility of the electrons across the axial magnetic field. In order to draw a radial current the radial electric field is thus strengthened to the point where any ions that are produced in the anode sheath are accelerated through the radial potential drop and thus can conduct an appreciable fraction of the current. This ion energy, which is gained directly from the radial electric field, appears as rotational energy of the ions due to the turning effect of the axial magnetic field. The first effect of the Hall currents is thus to produce a radial electric field and to make possible ion conduction so that momentum and energy can be transferred directly from the electromagnetic field into the azimuthal motion of the ions. Because of the centrifugal force on the ions they will never spin up to an azimuthal velocity as high as that of the electrons, which is probably quite close to the local value of $\left|\frac{E_r}{B_z}\right|$. This insures that Hall currents will always flow, even when particle mean free paths are very large compared to the diameter of the jet. A second effect of the Hall currents upon the acceleration mechanisms occurs precisely because the electrons are spinning faster than the ions, i.e., azimuthal momentum is transferred from the electrons to the ions through collisons. This insures that the ion energy is greater than what it gains by dropping through the radial potential drop.

The fact that the Hall currents are responsible for putting the energy and momentum initially into ion rotation rather than into axial velocity should not deter us from considering the device as primarily a Hall current accelerator. Also, most of the observations and measurements made so far upon MPD arc devices can be explained through Hall currents producing the accelerations discussed above. For this reason, it is believed that an intensive analytic investigation based upon the action of the Hall currents is likely to be much more useful than attempts to develop other explanations for the performance capabilities of MPD arc devices.

4.2 Electrode Mechanisms

4.2.1 Cathode Mechanisms

The current can be carried into the cathode by either ion bombardment or electron emission. For the latter process to occur the cathode requires a heat source to "boil off" the electrons. In practical accelerators both processes are occurring simultaneously. However, in most cathode configurations it is likely that one process will be dominant and hence control the nature of the cathode attachment region. Care should be exercised in cathode design to insure that both mechanisms are not equally likely to occur, since unstable or oscillatory cathode attachment might happen.

Although criteria that can be used to identify the cathode mechanism are not well defined; the following shall be used.

1. If the attachment is diffuse, the process is dominated by ion bombardment.
2. If a point attachment occurs, the process is dominated by electron emission.

In our accelerators which have extended cylindrical cathodes, it is observed that the cathode attachment occurs on the outer cylindrical surface; hence it is dominated by ion bombardment. This ion bombardment energy is partly conducted away and partly used up in electron thermionic emission. Because of the geometry, most of the ion energy is conducted away and a large fraction of the current must be carried by the ions. Calculations indicate that the cathode power loss for this case is many times larger than for a point attachment cathode carrying the same current. Also, the ion current used to heat the cathode does not produce any thrust, hence the thrust per unit current for an ion bombardment cathode will be considerably lower than for a point attachment cathode used in a similar engine configuration. These considerations indicate that considerable effort should be made to develop a reliable point attachment cathode.

Considerable analysis has been made of some idealized models of accelerator cathodes. The important phenomena of electron emission, cathode heating, and cathode heat loss have all been incorporated into the analysis. It has been concluded that one of the most important aspects of the "stability" of the attachment is the radial equilibrium of the ions. In a point attachment, the self-magnetic forces can be quite large which accelerates the ions away from the cathode tip as the cathode jet expands. The ions are now moving against the electric field and will have an outward force exerted on them even though the net radial body force or pinch is radially inward. Investigations are being pursued to determine the conditions under which the ions can still be confined to form a stable, slowly expanding cathode jet emanating from a point attachment. It is felt that little more can be done at present from a purely analytic point of view and it is expected that the experimental program will be of most use in further explaining this interesting form of "retrograde" motion.

4.2.2 Cathode Heat Transfer Calculations

To improve the efficiency and lifetime of arc jet cathodes it is important to determine the mode of cathode arc attachment which results in the smallest power losses. Basically the problem may be divided into two categories: differences in the geometry of attachment, and differences in the form of the energy distribution over the surface of the attachment region.

A comparison is made between a cylindrical "ring" attachment and a "conical tip" attachment. The comparison is made assuming both regions pass the same total current and operate at the same surface temperature (e.g., the melting point of tungsten). The results (derived in Appendix B) indicate that the loss of power to the cathode cooling water is smaller for conical tip attachment than for ring attachment. The numerical value of the power ratio, P_{tip}/P_{ring},

depends upon the half-angle of the cone and the radius of the cathode. The results (see Fig. 13) show that for $\theta = 90^{o}$ (i.e., flat-ended cylinder), this ratio is less than 1/2 and for $\theta = 45^{o}$, it is less than 1/4. The analysis predicts a ratio of zero in the limit $\theta \rightarrow o$, but it is expected that the heat conduction model used is no longer valid in this situation since convective effects are certainly important for the case of a long, slender cone.

A comparison is also made between the two limiting cases of energy distribution over a cylindrical attachment region; namely, a delta function energy input (i.e., a "ring" attachment of infinitesimal thickness), and a uniform energy input over the entire surface. These are chosen because the equations are easily solved and, presumably, the actual physical situation must be somewhere between these limits.

It can be shown in a reasonably general manner (see Appendix B) that the power loss for the delta function distribution is less than that for the uniform distribution. The exact power ratio, $P_{delta}/P_{uniform}$, depends upon the applied arc potential, the surface work function and a complicated integral involving the uniform energy distribution. A rough approximation of this integral indicates that the power loss for the delta function case can be considerably smaller than that for the uniform case under typical arc jet conditions.

These results therefore indicate that the best possible cathode attachment mode is a point attachment on a conical cathode. Previous experimental results (Subsection 3.3) appear to confirm these conclusions.

4.2.3 Anode Attachment

Investigations are being made to determine the relation between the anode attachment and the ionization phenomena. The possibility of producing a significant percentage of the ions inside of the anode is being studied. If the anode is run hot, e.g.,

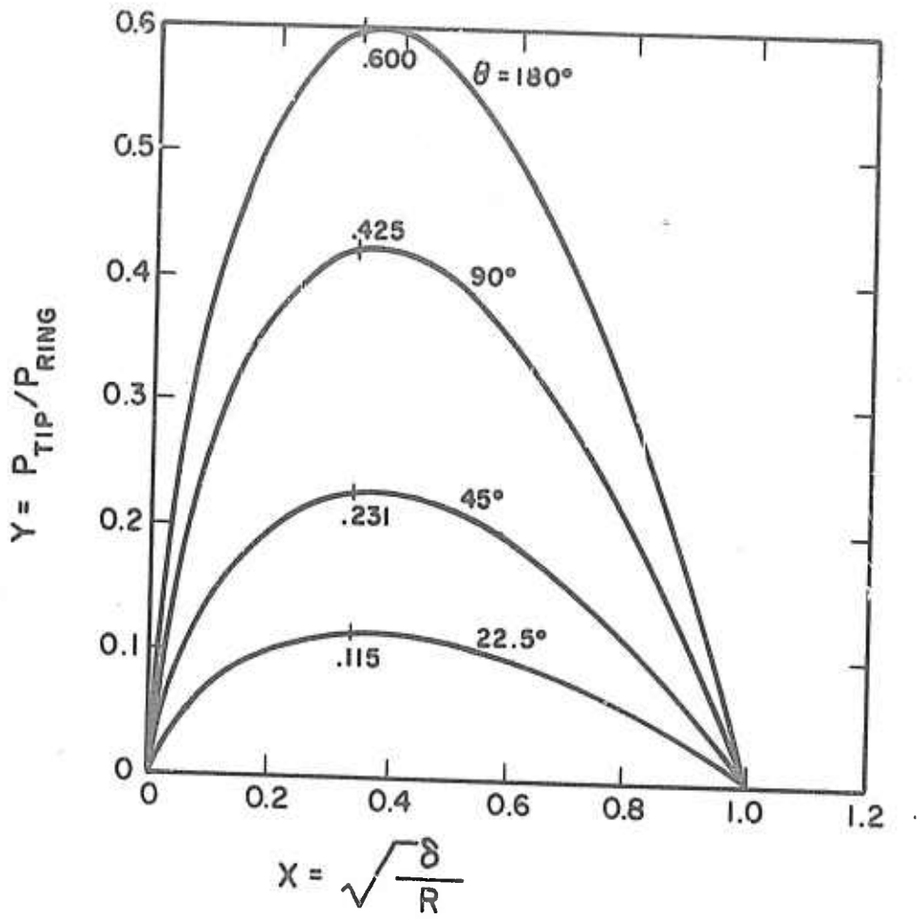

FIG. 13 COMPARISON OF RING AND TIP CATHODE ATTACHMENTS

about 3000°K near the attachment region, it is possible to create a reasonable equilibrium ionization level in the propellant vapor as it passes through the anode. If the passage is placed parallel to the magnetic field, then the ions can be exhausted from the anode with the propellant.

An expression for the anode heat loss has been derived which depends upon the gas properties and the specific impulse at which the engine is being operated.

Using a simple model of the anode sheath it is possible to derive the following expression for the power loss to the anode

$$P_A = \frac{10}{3} \frac{T}{\Psi} \bar{w}$$

where

T = thrust

$$\Psi = \frac{|e|\dot{m}}{m_a I}$$

$\bar{w}$ = average axial velocity of the gas near the anode.

This expression exhibits most of the characteristics observed for the anode power loss, provided that Ψ is interpreted as the "effective" value of Ψ.

5. IMPROVEMENTS OF MEASUREMENT TECHNIQUES

During the reporting period several steps have been made toward improving the accuracy, reliability and ease of operation of the propellant feed system and thrust measurement system (thrust balance). The accuracy objective is the achievement of 2 percent or less probable error in the measurements of thrust and propellant mass-flow-rate. These efforts and the results obtained to date are presented below. Additionally a feed system of much larger capacity is needed for endurance tests scheduled for early 1966. For the high-capacity system the present design will not be adequate; thus, a modified concept discussed below is now being designed.

5.1 Feed System Calibration

The bellows feed system calibration included a measurement of the effective displacement area of the bellows as a function of its length, determination of the rate of change of the bellows volume with respect to pressure differential (i.e., actuator force), and a measurement of the bellows spring force as a function of its length. These calibrations used the apparatus described in Ref. 4. The necessity of these measurements is evident from the following equation which expresses the mass-flow-rate of propellant leaving the bellows.

$$\dot{m} = \frac{dm}{dt} = \rho \left(\frac{\partial V}{\partial x}\right) \frac{dx}{dt} + \rho \left(\frac{\partial V}{\partial F^*}\right) \frac{dF^*}{dt} + V \left(\frac{\partial \rho}{\partial T}\right) \frac{dT}{dt} \qquad (4)$$

where

m = mass in bellows

x = $(L_{max} - L)$ = displacement of bellows

V = $V(x, F^*)$ = volume of bellows

ρ = density of liquid in bellows

T = temperature of liquid in bellows

t = time

$F^* = F_A - F_S$ = (bellows actuator force) - (bellows spring force)

The first term is the principal term and the coefficient $(\frac{\partial V}{\partial x})$ is the effective piston area of the bellows. The second term is due to the deflection of the convolutions of the bellows under the pressure force. The third term represents the effect of thermal expansion (primarily of the propellant).

The second term expands to:

$$\rho \left(\frac{\partial V}{\partial F^*}\right) \left(\frac{dF_a}{dt} + \frac{dF_s}{dx} \cdot \frac{dx}{dt}\right)$$

The factors determined by calibration were:

$\frac{\partial V}{\partial x}$ = effective piston area

$\frac{\partial V}{\partial F^*}$ = volume displacement due to pressure differential

$\frac{dF_s}{dx}$ = bellows spring constant

The flow rate is measured by measuring the actuation rate, dx/dt, and the actuator force rate dF_a/dt. The force rate is measured from a strip chart recording of the output of the actuator force transducer. It should be noted that the force rate term is a "correction" term - usually small compared to the first term. The thermal expansion term is kept small by precise control of the temperature - accomplished with the aid of a two-phase tin constant-temperature bath surrounding the feed system.

Figures 14, 15, and 16 show the calibration results in terms of volume as a function of displacement, volume change as a function of actuator force, and spring force as a function of displacement. Note that near the fully-compressed position all of these become nonlinear. For best accuracy this nonlinear region should not be used in testing. The calibration factors have been determined to an accuracy of 2 percent or better.

5.2 Vaporizer for Bellows Feed System

The function of the vaporizer is to localize and stabilize the process of evaporation which must occur as the liquid flows from the feed system into the arc. Previous work made no special provisions to control the location of vaporization but depended upon the liquid vaporizing as it flowed into the "hot" anode. This had the advantage of simplicity and more effective regenerative cooling. However, the vaporization was frequently unstable and the flow into the arc would pulsate. An additional bad feature of vaporization in the anode was the frequent occurrence of "flooding" at the beginning of runs when an excessive amount of liquid would flow into the space between cathode and anode.

These difficulties have been essentially overcome by the vaporizer shown in Fig. 17. The essential feature of this vaporizer is a steep temperature gradient which localizes and stabilizes the vapor front in the porous plug. The temperature gradient results from the heating coils located on the upper end, the low heat conductance of the tube-porous-plug assembly, and the radiation from the exposed, unheated section of the vaporizer.

Another feature of this system is that it operates at a low pressure (a few psi). Thus, changes and rates of change of pressure with respect to time are low, and the force-rate correction term (second term in Eq. 4) is small. This enhances the accuracy of mass-flow-rate measurements.

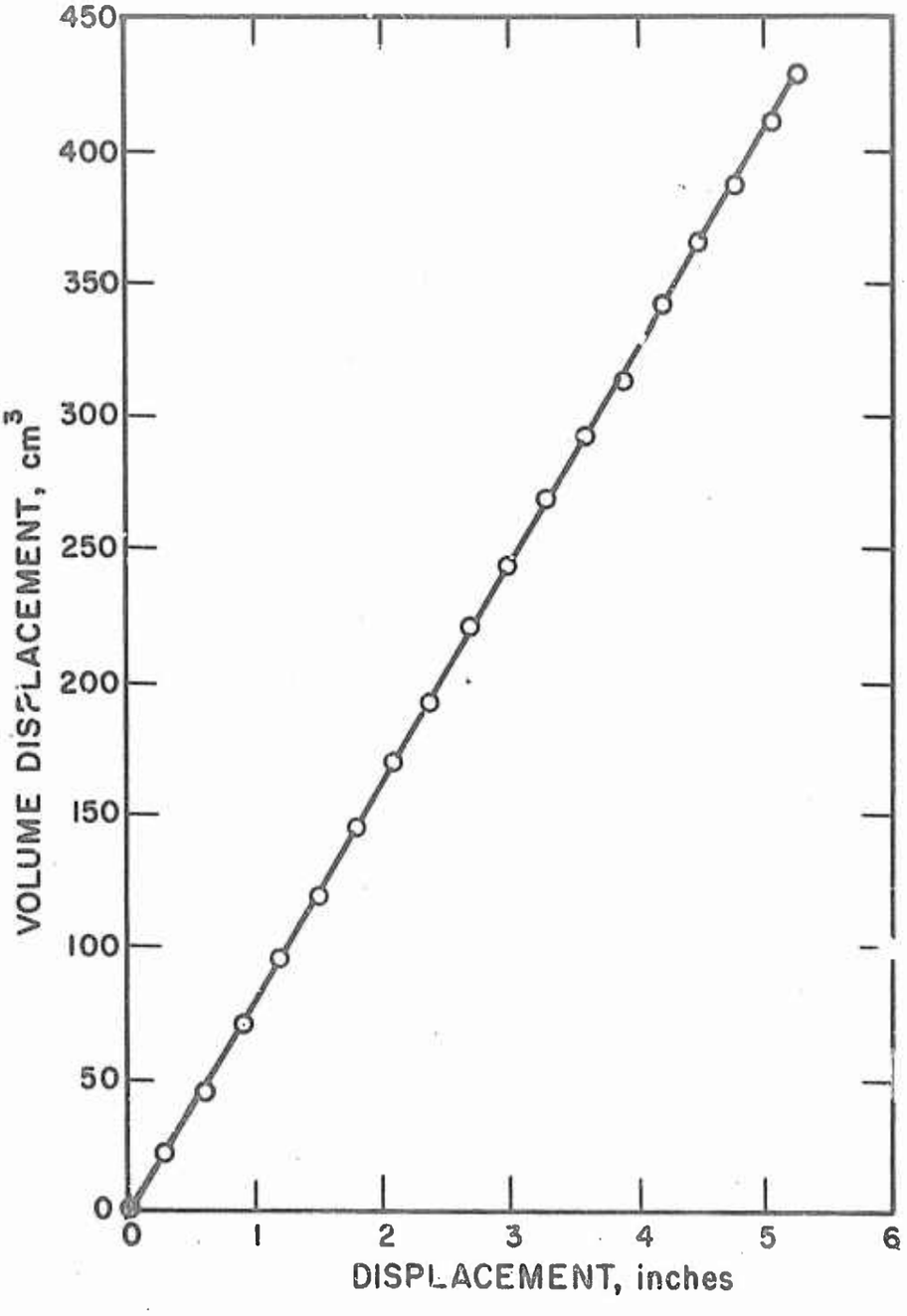

FIG. 14 FEED SYSTEM BELLOWS — VOLUME DISPLACEMENT VERSUS LINEAR DISPLACEMENT

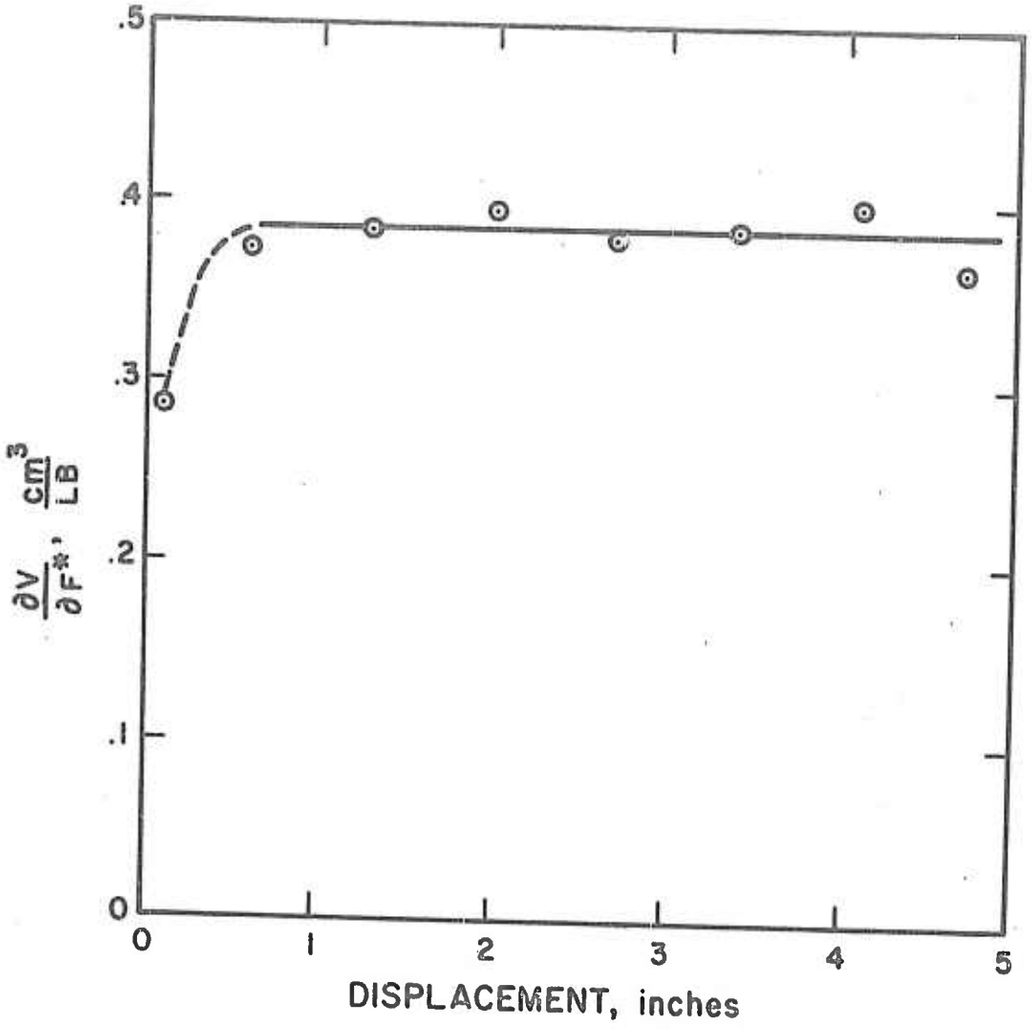

FIG. 15 FEED SYSTEM BELLOWS — VOLUME CHANGE DUE TO PRESSURE DIFFERENCE

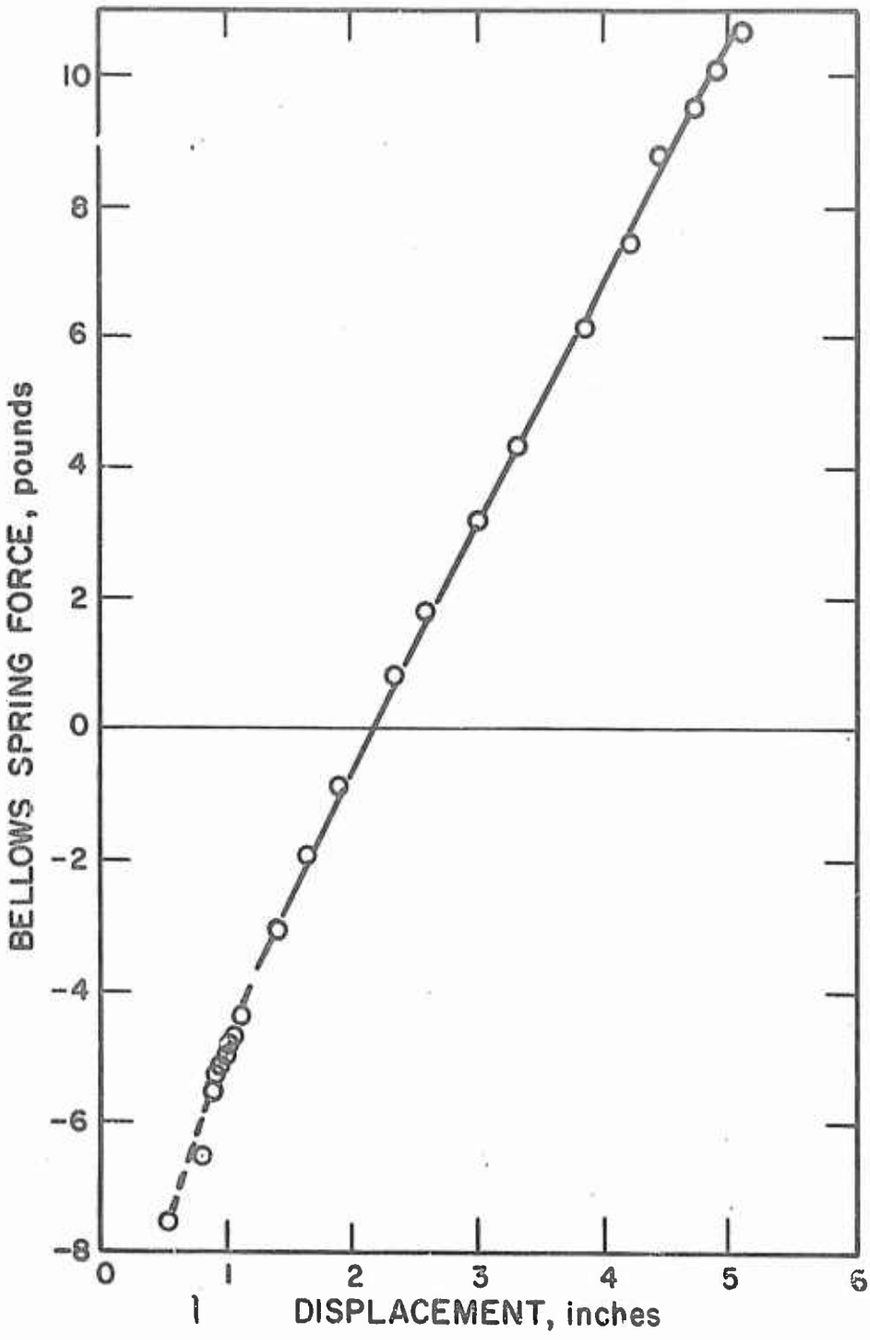

FIG. 16 FEED SYSTEM BELLOWS SPRING FORCE CALIBRATION

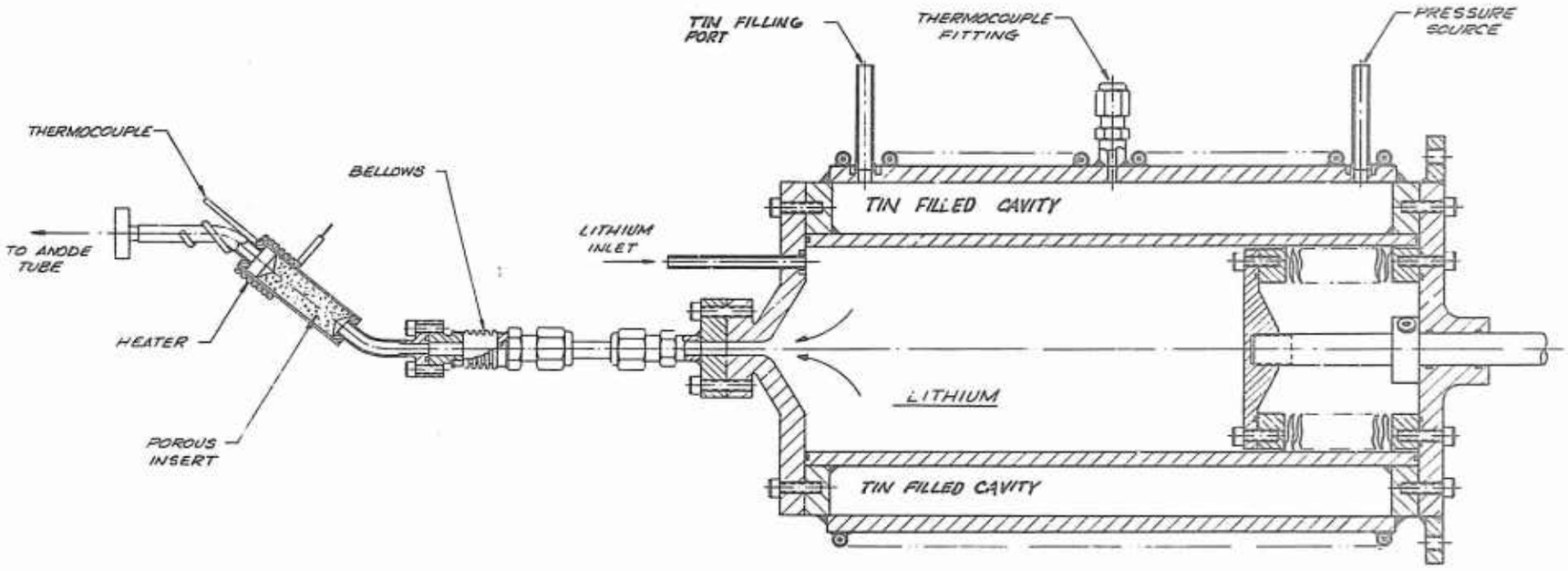

FIG. 17 MK-1B LITHIUM FEED SYSTEM AND VAPORIZER

5.3 High-Capacity Feed System

Design and evaluation of a high-capacity feed system which will be needed for the 50-hour endurance tests scheduled for early 1966 have been started. This system, as Fig. 18 shows, would consist of a bellows-type propellant reservoir, a boiler, a critical orifice, and related controllers. In this design the flow is metered in the vapor state (rather than in the liquid state) by measuring the stagnation pressure and temperature of the flow through the critical orifice. The flow rate will be proportional to the pressure and inversely proportional to the square-root of the stagnation temperature of the vapor at the orifice. The vapor leaves the boiler in a saturated vapor state at the vapor pressure corresponding to the temperature of the liquid in the boiler. It is necessary to "super-heat" the vapor before it reaches the orifice to avoid condensation as it expands through the orifice.

As the propellant vaporizes and flows out of the boiler, the bellows would be displaced and more liquid would flow into the boiler to maintain a constant level of the liquid. The bellows control system would be governed by the liquid level sensor, which will probably be a resistor immersed in the liquid. Although precise liquid level sensing and control is difficult with an alkali metal, it should be relatively straightforward in this system because the level is not critical and could be allowed to vary over a relatively large distance (say 50 percent of the boiler depth).

The boiler control will regulate the boiler-heater current to maintain the pressure (indicated by the pressure transducer) equal to the set-point pressure. This pressure transducer is the key component in the system. It must be compatible with the alkali metals at temperature slightly above the melting points. Note that the transducer will be located far enough away from the boiler that it will not be subjected to the higher boiler temperatures. Two manufacturers of transducers which may be suitable for this application are Mine Safety Appliances Company (Research Division) and Consolidated Electrodynamics Corporation.

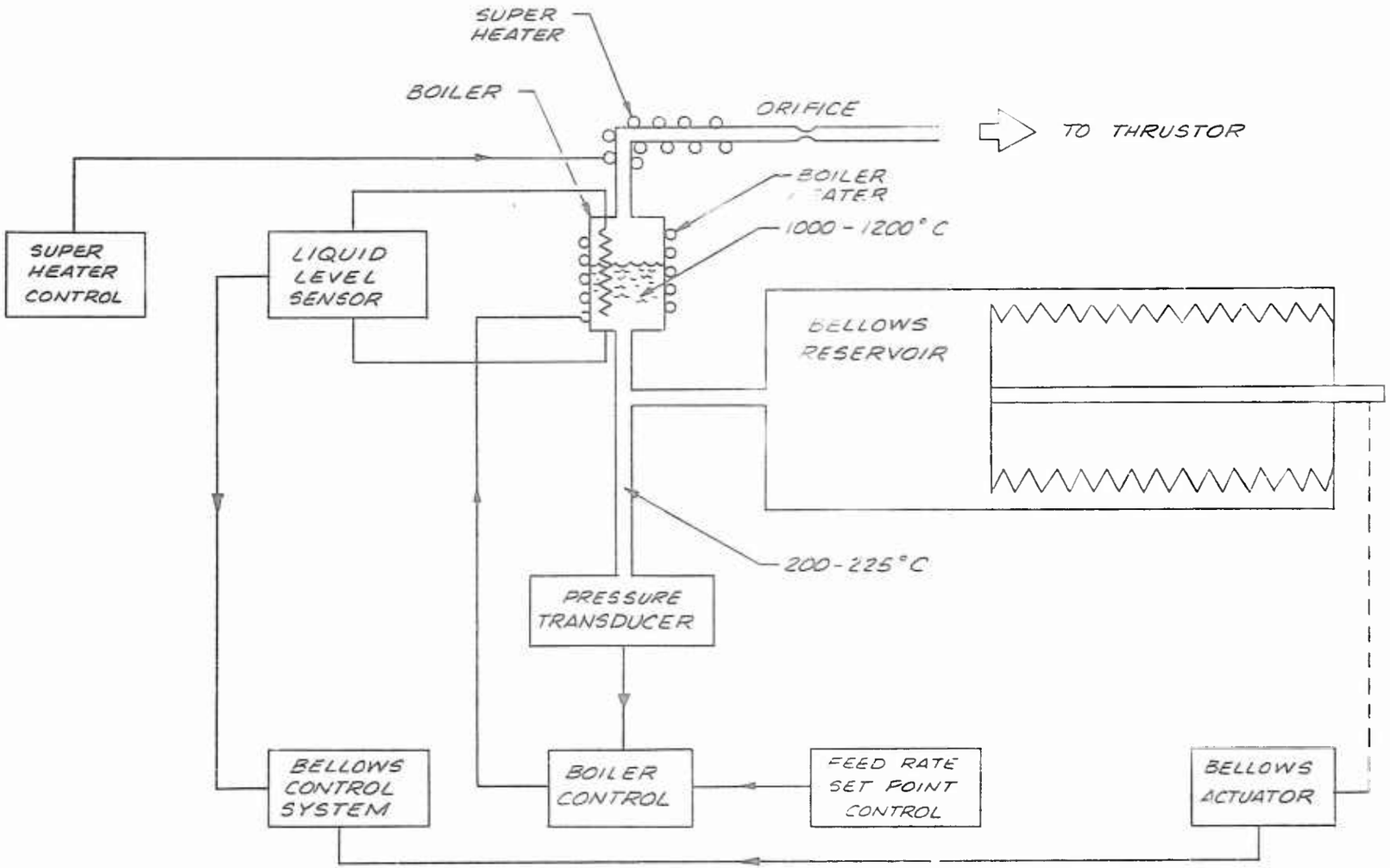

FIG. 18 HIGH CAPACITY ALKALI METAL FEED SYSTEM

Instead of measuring the pressure directly the flow could be determined by measuring the temperature of the liquid since it is in the saturated-liquid state. However, because of the exponential relationship between temperature and vapor pressure the accuracy of this method is very poor. Our error analysis showed that the temperature measurement has to be within 0.05 percent if the flow-rate is to be within 2 percent. This temperature measurement accuracy is difficult if not impossible to achieve in the type of experiments being conducted.

This system has advantages over either a large boiler or a large bellows feed system. The accuracy problems with a large bellows have already been mentioned. A large boiler would be very expensive to fabricate since it has to be made out of a refractory metal and the heater power requirements would be very large.

5.4 Thrust Balance Improvements

Efforts to improve the accuracy of thrust measurement are concentrated on:

1. Reduction of tare forces due to the interaction between the applied magnetic field and current leads.
2. Reduction of forces caused by cooling-water pressure, flow and temperature changes.

The effects of the magnitude and variation of these forces are the principal sources of error in a thrust measurement.

To reduce the electromagnetic tare forces, the power lines to the thrustor electrodes and the magnet coil will be transmitted across the balance coaxially. As in previous balance designs, the power connections across the balance are made through mercury to avoid interference of rigid power cables. Two coaxial mercury pots were designed, fabricated, tested, and incorporated into the existing balance during the reporting period. Figure 19 shows a sketch of the coaxial mercury pot design.

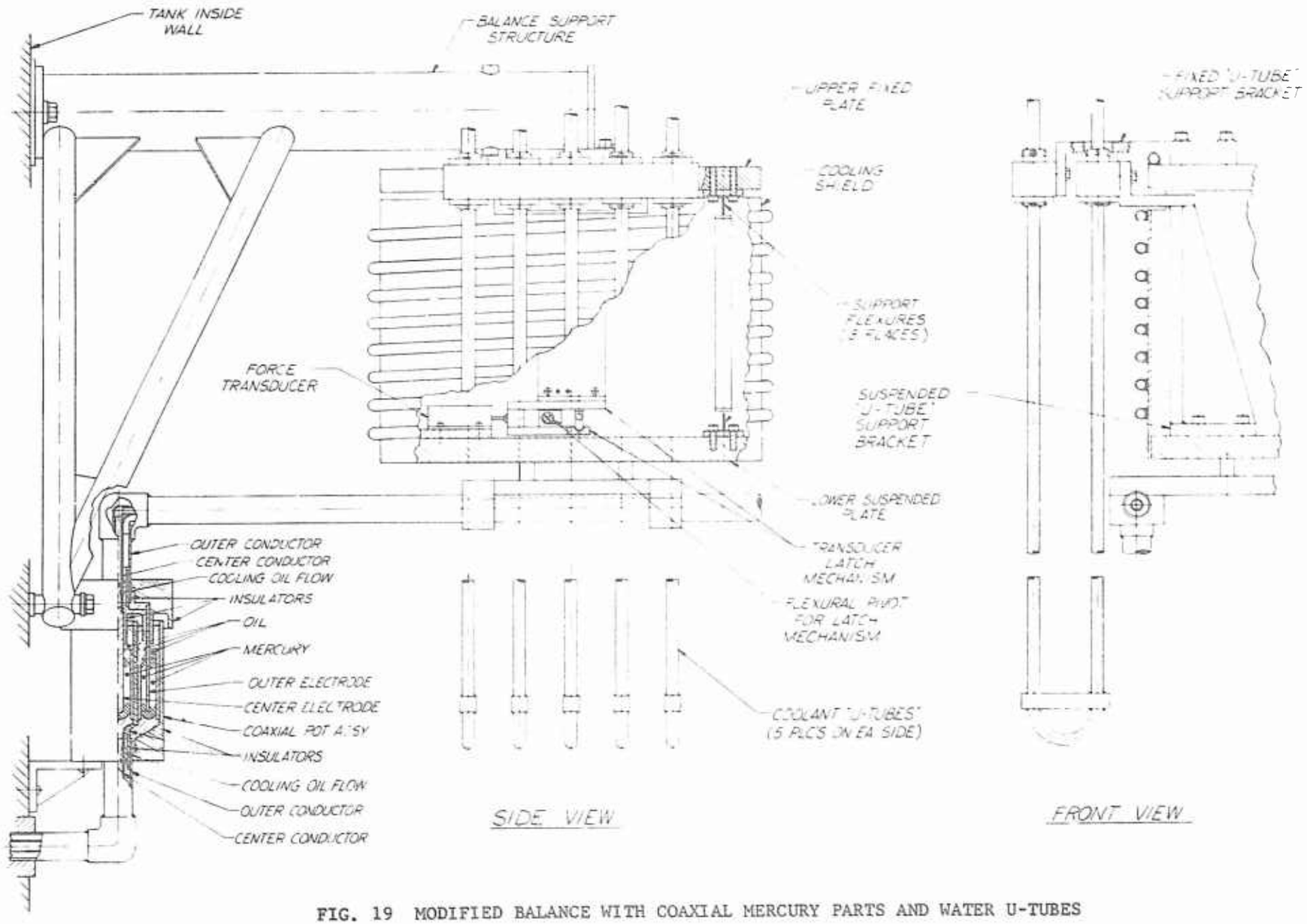

FIG. 19 MODIFIED BALANCE WITH COAXIAL MERCURY PARTS AND WATER U-TUBES

For reduction of the forces caused by coolant flow across the balance the U-tube arrangement shown in Fig. 19 has been adopted. The U-tube concept allows thermal expansion of a metal tube without a force on the balance by connecting the ends of the tube at the same vertical position - one side to the suspended balance platform and the other side to the fixed balance support. Bench tests showed that the relative position between the inlet and outlet of the tube did not shift measurably (less than 5×10^{-4} in.) with changing temperature and pressure in the tube. Subsequent tests of a single coolant circuit (two U-tubes) mounted temporarily on the balance showed that the maximum force due to water pressure and flow was about one gram. Five such circuits (10 U-tubes) are now being permanently mounted on the existing balance along with the coaxial mercury pots.

REFERENCES

1. High Specific Impulse Thermo-Ionic Acceleration, Giannini Scientific Corp., Report No. RRE-114-a, Santa Ana, California, Dec 1963

2. G. L. Cann, Thermal Arc Jet Research, EOS Report 3810-ML-11, Contract No. AF 33(657)-10789, 15 Feb 1964

3. R. A. Moore, G. L. Cann, et al, Thermal Arc Jet Research, TDR No. APL-TDR-64-55, Air Force Aero Propulsion Laboratory, May 1964

4. R. A. Moore, G. L. Cann, et al, High Specific Impulse Thermal Arc Jet Thrustor Technology, Air Force Aero Propulsion Laboratory Report AFAPL-TR-65-48, Part I, June 1965

5. S. Bennett, G. Enos, R. R. John, A. Tuchman, MPD Arc Jet Engine Performance, AIAA Paper 65-296, presented at AIAA Second Annual Meeting, San Francisco, July 26-29, 1965

6. Design and Development of a Thermo-Ionic Electric Thrustor, Giannini Scientific Corp., Report No. 4QS055-968, Santa Ana, California, May 1965

7. G. L. Cann, P. D. Lenn, R. L. Harder, Hall Current Accelerator EOS Report 5470-Q-2, Contract NAS3-5909, 20 Dec 1964

8. G. L. Cann, P. D. Lenn, R. L. Harder, Hall Current Accelerator EOS Report 5470-Q-3, Contract NAS3-5909, 20 Mar 1965

9. G. L. Cann, R. L. Harder, Study of Electrode Attachment Regions in High-Current Gaseous Discharges, Arnold Engineering Development Center Report AEDC-TDR-64-107, Aug 1964

APPENDIX A

TEST DATA

Thrustor Model: LAJ-AF-6D

Propellant: Potassium

Test Chamber: 6' x 6'

Run No.	Point No.	I_A amps	V_A volts	P_A kw	I_C amps	$\dot{m}$ gm/sec	p_t torr	P_{cath} kw	P_{an} kw	P_{TK} kw	T grams	I_{sp} sec	η_o -
679	1	300	36.0	10.8	1800	0.0400	9.2×10^{-4}	1.31	1.60	3.27	50.6	1270	0.277
	2	300	39.5	11.9	1800	0.0320	4×10^{-4}	1.25	3.06	6.65	46.7	1460	0.276
	A	300	39.0	11.7	1800	0.0410	-	-	-	-	48.2	1180	0.232
	B	300	37.5	11.3	1800	0.0420	-	-	-	-	56.8	1350	0.328
680	1	200	28.0	5.60	1800	0.0430	3×10^{-4}	0.79	1.36	2.33	30.0	700	0.179
	2	300	36.5	11.0	1800	0.0440	2×10^{-4}	1.04	2.13	3.02	50.0	1140	0.249
	3	300	37.5	11.3	1800	0.0460	2×10^{-4}	1.15	2.87	4.94	50.2	1090	0.234
	A	200	38.5	7.70	1800	0.0580	-	-	-	-	33.2	570	0.118
	B	300	36.0	10.8	1200	-	-	-	-	-	-	-	-
	C	200	32.0	6.40	1200	0.0310	-	-	-	-	-	-	-
681	A	158	32.0	5.06	1800	0.0325	3.4×10^{-4}	0.82	1.48	2.68	26.6	820	0.207
	B	155	33.0	5.11	1800	0.0325	3.4×10^{-4}	0.82	1.48	2.68	26.2	808	0.199
	C	250	39.5	9.88	1800	0.0330	3.0×10^{-4}	1.11	2.34	3.22	43.0	1300	0.274
	D	250	40.0	10.0	1800	0.0333	2.6×10^{-4}	1.21	2.68	4.02	41.8	1260	0.253
	E	250	40.5	10.1	1800	0.0336	2.6×10^{-4}	1.21	2.68	4.02	43.0	1280	0.262
	F	250	36.0	9.00	1600	0.0336	2.6×10^{-4}	1.23	2.96	4.83	43.0	1280	0.294
	G	250	36.0	9.00	1600	0.0342	2.6×10^{-4}	1.23	2.96	4.83	42.2	1240	0.280
	H	250	32.5	8.13	1400	0.0342	2.4×10^{-4}	1.19	2.76	4.83	38.0	1110	0.250
	I	250	32.5	8.13	1400	0.0345	2.4×10^{-4}	1	[illegible]	4.83	36.2	1050	0.225
	J	250	29.0	7.25	1200	0.0346	2.4×10^{-4}			4.56	35.0	1010	0.235
	K	250	29.5	7.38	1200	0.0345	2.3×10^{-4}	1.		4.56	34.3	995	0.221

Page 2.

Thrustor Model: LAJ-AF-6D

Propellant: Potassium

Test Chamber: 6' x 6'

Run No.	Point No.	I_A amps	V_A volts	P_A kw	I_C amps	$\dot{m}$ gm/sec	p_t torr	P_{cath} kw	P_{an} kw	P_{TK} kw	T grams	I_{sp} sec	η_o -
681	L	250	26.5	6.63	1000	0.0347	2.6×10^{-4}	1.10	2.28	4.02	32.6	940	0.222
	M	250	26.3	6.56	1000	0.0351	2.6×10^{-4}	1.10	2.28	4.02	32.0	911	0.214
	N	250	24.0	6.00	800	0.0350	2.6×10^{-4}	1.13	2.03	3.75	29.7	850	0.203
	O	250	24.5	6.12	800	0.0350	2.6×10^{-4}	1.13	2.03	3.75	29.7	850	0.198
	P	250	38.5	9.62	1800	0.0350	1.8×10^{-4}	1.16	2.54	3.62	43.4	1240	0.268
	Q	250	38.5	9.62	1800	0.0348	1.8×10^{-4}	1.16	2.54	3.62	43.5	1250	0.272
	R	250	46.0	11.5	1800	0.0209	2.2×10^{-4}	1.49	4.23	5.50	35.3	1690	0.249
	S	250	46.0	11.5	1800	0.0209	2.4×10^{-4}	1.49	4.23	5.50	35.3	1690	0.249
	T	200	41.5	8.30	1800	0.0210	2.0×10^{-4}	1.33	3.48	5.87	31.2	1480	0.267
	U	195	42.0	8.20	1800	0.0211	2.0×10^{-4}	1.33	3.48	5.87	31.3	1480	0.271
	V	158	37.3	5.89	1800	0.0213	2.0×10^{-4}	1.01	2.25	5.36	26.4	1240	0.267
	W	154	38.0	5.85	1800	0.0213	2.0×10^{-4}	1.01	2.25	5.36	26.5	1240	0.265
	X	100	31.0	3.10	1800	0.0213	2.8×10^{-4}	0.81	1.44	3.86	14.7	690	0.157
	Y	100	30.5	3.05	1800	0.0213	2.8×10^{-4}	0.76	1.23	2.52	15.3	719	0.170
	Z	100	38.5	3.85	1800	0.0213	2.6×10^{-4}	-	-	-	15.4	1480	0.284

APPENDIX B

CATHODE HEAT TRANSFER CALCULATIONS

Case I

Comparison of Power Losses for Cylindrical "Ring" vs Conical "Tip" Arc Attachment Modes.

From Fig. B-1, it can be seen that, provided the half-width of the attachment "ring" is small with respect to the radius of the cylinder, the problem may be approximately "unwrapped" into a "trough" on a flat plate of thickness R, width $2\pi R$ and infinite length.

The steady-state heat conduction equation in the absence of sources or sinks is given by

$$\nabla^2 \phi = 0$$

where

$\phi \equiv \int k \, dT$

k = thermal conductivity of the cathode material

T = temperature

In the cylindrical geometry of Fig. B-2 this becomes

$$\frac{1}{r} \frac{d}{dr} \left[r \frac{d\phi}{dr} \right] = 0$$

or

$$r \frac{d\phi}{dr} = -\lambda \qquad \lambda = \text{constant}$$

and

$$\phi = -\lambda \ln r + C_1$$

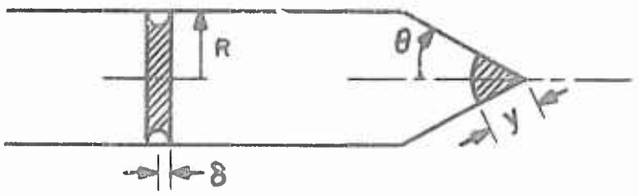

FIG. B-1 GEOMETRY OF "RING" AND "TIP" CATHODE ATTACHMENTS

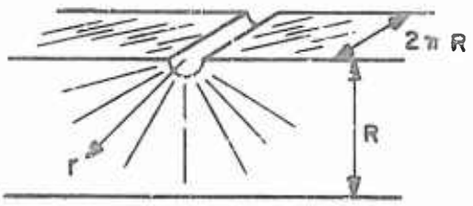

FIG. B-2 GEOMETRY OF "UNWRAPPED" RING ATTACHMENT

The boundary conditions $\phi = \phi_o$ at $r = \delta$ and $\phi = \phi_\infty$ at $r = R$ give

$$\phi_o - \phi_\infty = \lambda \ln (R/\delta)$$

The heat flux q is given by

$$q = -\frac{d\phi}{dr} = \frac{\lambda}{r}$$

or

$$q = \frac{\phi_o - \phi_\infty}{r \ln (R/\delta)}$$

and

$$q\Big|_{r = \delta} = (\phi_o - \phi_\infty)/\delta \ln (R/\delta)$$

The power is given by $P_{ring} = q_{ring} A_{ring}$ where $q_{ring} = q\Big|_{r = \delta}$ and $A_{ring} = 2\pi^2 R\delta$. Thus

$$P_{ring} = 2\pi^2 R (\phi_o - \phi_\infty)/\ln (R/\delta)$$

Now, for the conical tip problem we write $\nabla^2\phi$ in spherical polar coordinates and obtain

$$\frac{1}{r^2} \frac{d}{dr} \left[r^2 \frac{d\phi}{dr}\right] = 0$$

or

$$r^2 \frac{d\phi}{dr} = -\beta$$

or

$$\phi = \frac{\beta}{r} + C$$

Applying the boundary conditions $\phi = \phi_o$ at $r = y$ and $\phi = \phi_\infty$ at $r = \infty$ we find

$$\phi_o - \phi_\infty = \beta/y$$

The heat flux is given by $q = -\frac{d\phi}{dr} = \frac{\beta}{r^2}$ and $q\,|_{r = y} = \frac{\beta}{y^2} = \frac{\phi_o - \phi_\infty}{y}$. The power is given by $P_{tip} = q_{tip} A_{tip}$, where $q_{tip} = q\,|_{r = y}$ and A_{tip} is the spherical cap area which can be determined from the integral

$$A_{tip} = \int_o^\theta \int_o^{2\pi} (y\, d\theta)(y \sin\theta\, d\varphi) = 2\pi\, y^2 [1 - \cos\theta]$$

Hence

$$P_{tip} = 2\pi y (\phi_o - \phi_\infty) [1 - \cos\theta]$$

Further,

$$I_{tip} = I_{ring} = I$$

and

$$\phi_{o\ tip} = \phi_{o\ ring} \text{ (corresponding to the melting point).}$$

Provided the current density is primarily due to thermionic emission the conditions above result in equal current densities and therefore equal emitting areas for the ring and the conical tip

cases. Assuming that the tip melts back to the point where the spherical cap is at the melting point, then

$$2\pi^2 R\delta = 2\pi y^2 (1 - \cos\theta)$$

or

$$y/R = \sqrt{\frac{\delta}{R} \frac{\pi}{1 - \cos\theta}}$$

Thus

$$\frac{P_{tip}}{P_{ring}} = \frac{\delta/R}{y/R} \ln (R/\delta)$$

Noting that

$$\sqrt{\frac{1 - \cos\theta}{2}} = \sin\left(\frac{\theta}{2}\right)$$

We find

$$\frac{P_{tip}}{P_{ring}} = \sqrt{\frac{8}{\pi}} \sin\left(\frac{\theta}{2}\right) X \ln\left(\frac{1}{X}\right)$$

where

$$X^2 \equiv \delta/R < 1$$

The ratio P_{tip}/P_{ring} is shown in Fig. 13 for various values of X and θ. In all cases the ratio is less than unity and decreases with decreasing θ. This indicates that within the framework of our assumptions the power loss from a conical attachment is always less than that from a ring attachment.

Case II

Comparison of Delta Function and Uniform Surface Energy Distributions. For a cylinder of radius R and length L with an energy input Q(z) per unit area, and essentially one-dimensional heat conduction, we obtain the differential equation

$$\frac{d^2T}{dz^2} = \frac{2Q(z)}{RK}$$

where

$$Q(z) = V\, j_i(z) - \chi\, j_e(z)$$

Physically this implies that the ion current density j_i arrives at the surface of the cathode with the arc voltage V while an electron current density j_e leaves the surface with the work function, χ, of the cathode material.

The Richardson equation for thermionic emission may be written in the form

$$j_e = j_o\,(T/T_{max})^2\, e^{-\varepsilon\chi/kT}$$

The total current, which is to be regarded as constant, is given by

$$I_o = 2\pi R \int_o^L [j_i(z) + j_e(z)]\, dz$$

the net power into the cathode, from the ions, is given by

$$P = 2\pi RV \int_o^L j_i(z)\, dz$$

For the case of a Delta function heat source we take

$$Q(z) = \delta(z)$$

which yields

$$T = C_1 z + C_2$$

The boundary conditions are $T(o) = T_{max}$ and $T(L) = 0$. We define $\theta \equiv T/T_{max}$ and $\xi \equiv z/L$.

The temperature distribution is just $\theta = 1 - \xi$ and

$$j_e = j_o (1 - \xi)^2 e^{-B/(1 - \xi)} \qquad B \equiv e\chi/kT_{max}$$

Now, for $z \neq 0$, $Q(z) = 0$ and $j_i(z) = \frac{\chi}{V} j_e(z)$

Thus $I_o = 2\pi RL\, j_o (1 + \chi/V)\, \mathcal{R}(B)$

where $\mathcal{R}(B) \equiv \int_o^1 (1 - \xi)^2 e^{-B/(1 - \xi)}\, d\xi$

also, $P_{delta} = 2\pi R \int_o^L V\, j_i(z)\, dz$

$= 2\pi RL\chi\, j_o\, \mathcal{R}(B)$

Substituting for $\mathcal{R}(B)$ from the above current relation we obtain

$$P_{delta} = I_o V \left[\frac{\chi}{V + \chi}\right]$$

For the case of a uniform heat source we take

$$Q(z) = Q_o = \text{constant}$$

then

$$\frac{d^2T}{dz^2} = A_o \qquad A_o \equiv \frac{2Q_o}{RK_o}$$

Applying the same boundary conditions and dimensionless variables we find for the temperature distribution

$$\theta = (1 - \xi)(1 - \alpha\xi) \qquad \alpha \equiv A_o L^2/2T_{max}$$

and

$$j_e = j_o \theta^2 e^{-B/\theta}$$

$$j_i = \frac{\chi}{V} j_e + \frac{Q_o}{V}$$

$$I_o = 2\pi R \int_o^L \left(j_i(z) + j_e(z)\right) dz'$$

$$= 2\pi RL \left[\frac{Q_o}{V} + \left(\frac{V + \chi}{V}\right) j_o \mathcal{L}(\alpha, B)\right]$$

where

$$\mathcal{L}(\alpha, B) \equiv \int_o^1 (1 - \xi)^2(1 - \alpha\xi)^2 e^{-B/(1 - \xi)(1 - \alpha\xi)} d\xi$$

and

$$P_{uniform} = 2\pi R \int_o^L V j_i(z) dz$$

$$= 2\pi RV \int_o^L \left[\frac{\chi}{V} j_e(z) + \frac{Q_o}{V}\right] dz$$

$$= 2\pi R\chi \int_o^L j_e(z)dz + 2\pi RLQ_o$$

and

$$\int_0^L j_e(z)\, dz \equiv j_o L \mathcal{L}(\alpha, B)$$

thus

$$P_{uniform} = 2\pi RL [\chi j_o \mathcal{L} + Q_o]$$

$$= I_o V \left[\frac{\chi}{\chi + \frac{V}{1+\beta}} \right]$$

where

$$\beta \equiv \frac{Q_o}{\chi j_o \mathcal{L}(\alpha, B)} > 0$$

Therefore

$$\frac{P_{uniform}}{P_{delta}} = \frac{\chi + V}{\chi + \frac{V}{1+\beta}} \geq 1 \text{ for } \beta \geq 0$$

Hence the delta function will, other things being equal, result in a smaller power loss than a uniform energy distribution. This is a general result which can be expected to apply within the framework of the assumptions. In order to obtain numerical values for the power ratio, $P_{uniform}/P_{delta}$, we must estimate β.

We can obtain a very rough value for β by replacing $e^{-B/(1-\alpha\xi)(1-\xi)}$ by $e^{-B[1-\xi]^{2n}}$ which is equivalent to setting $\alpha = 1$ and replacing the exponential function by a polynomial adjusted to a "best-fit" through the proper choice of n. It now follows that

$$\mathcal{L}(1, B) = \int_0^1 (1 - \xi)^4 \, e^{-B} \, (1 - \xi)^{2n} \, d\xi$$

$$= e^{-B} \left. \frac{(1 - \xi)^{2n+5}}{2n + 5} \right|_0^1 = \frac{e^{-B}}{2n + 5}$$

By comparison with a plot of $e^{-1/(1 - \xi)^2}$ it is found that $n \approx 20$. Hence

$$\mathcal{L}(1, B) = \frac{1}{45e^B}$$

and

$$\beta = \frac{45e^B \, Q_o}{\chi \, j_o}$$

Further, within the spirit of the previous approximation we may take

$$\frac{Q_o}{\chi \, j_e} = \frac{V}{\chi} \quad \frac{j_i}{j_e} \quad - 1 = 0(1)$$

and

$$B = e\chi/kT_{max} \approx 5$$

hence

$$\beta \approx 0(10^4)$$

While the approximations are admitted quite rough, it is clear that $\beta \gg 1$ and in this limit, provided $\beta \chi/V \gg 1$ (i.e., provided $\chi \neq o$ and V finite) then

$$\lim_{\beta \to \infty} \left[\frac{P_{uniform}}{P_{delta}} \right] = 1 + \frac{V}{\chi}$$